aerospace

MDPI

Review

Combustion Behaviour of ADN-Based Green Solid Propellant with Metal Additives: A Comprehensive Review and Discussion

Rushikesh Kore [1,2] and Ashish Vashishtha [1,2,*]

[1] Department of Aerospace and Mechanical Engineering, South East Technological University (SETU), Carlow Campus, R93 V960 Carlow, Ireland
[2] The Centre of Research and Enterprise in Engineering (engCORE), South East Technological University (SETU), Carlow Campus, R93 V960 Carlow, Ireland
* Correspondence: ashish.vashishtha@setu.ie

Abstract: Solid propellants play a crucial role in various civil, scientific, and defence-related aerospace propulsion applications due to their efficient energy release, high energy density, low fabrication cost, and ease of operation. Ammonium dinitramide (ADN) has gained considerable attention as a potential oxidizer for green solid propellants due to its high oxygen content, significant energy density, non-toxicity, and non-polluting combustion products, leading to lower environmental impact. As ADN is a new desirable oxidizer in the field of solid propellants, understanding the practicality and viability of the use of ADN in composite solid propellants necessitates a thorough understanding of its chemical and thermal decomposition pathways in addition to its combustion characteristics in the presence of other ingredients. ADN is being explored as an alternative to the traditionally used ammonium perchlorate (AP), a toxic oxidizer containing chlorine (Cl). Additionally, AP monopropellants often suffer from moderate burning rates and poor mechanical strength. To address these limitations, researchers have explored the incorporation of metal additives, such as aluminium (Al), magnesium (Mg), and metalloid boron (B), to enhance the combustion performance and burn rate of AP. These metals not only act as energy-rich additives but also influence the combustion process through various mechanisms. The incorporation of metal additives into ADN has shown promising enhancements in the overall energetic performance of green solid propellants. This review aims to provide an in-depth analysis of the thermal decomposition of ADN and its combustion behaviour, along with the combustion of ADN-based solid propellants with metal additives. Finally, based on an extensive review of the existing literature, various research pathways for focused future collaborative efforts are identified to further advance ADN-based "green" solid propellants.

Keywords: green propellant; ammonium dinitramide (ADN); thermal decomposition; combustion; metallic fuels

Academic Editor: Fabrizio Ponti

Received: 23 October 2024
Revised: 5 January 2025
Accepted: 6 January 2025
Published: 12 January 2025

Citation: Kore, R.; Vashishtha, A. Combustion Behaviour of ADN-Based Green Solid Propellant with Metal Additives: A Comprehensive Review and Discussion. *Aerospace* **2025**, *12*, 46. https://doi.org/10.3390/aerospace12010046

1. Introduction

The quest for efficient and high-performance propulsion systems has been a driving force in the evolution of rocket systems in the past decades. Solid propellants, with their advantages of simplicity, controllability, and reliability, have played a pivotal role in various space missions, satellite launches, and military applications. Among the myriad solid propellant formulations, ammonium dinitramide (ADN) has emerged as a promising and innovative propellant ingredient, showcasing exceptional potential for enhancing the performance and safety of solid rocket propulsion systems along with a low environmental

impact. The discovery of ADN and its application to solid propellants is considered one of the important breakthroughs within the area of energetic materials. ADN was initially produced in 1971 at the Zelinsky Institute of Organic Chemistry, Moscow, USSR [1–5]. Over the years, researchers and scientists have tirelessly pursued the development of novel propellant formulations to meet the ever-increasing demands of modern aerospace endeavours. The advent of ADN, an ammonium salt of dinitraminic acid (HDN), has garnered substantial attention due to its enhanced performance characteristics (of high specific impulse and higher burning rate [6]), which make it an attractive alternative to traditional solid propellant oxidizers such as ammonium perchlorate (AP) and ammonium nitrate (AN). ADN's molecular structure, containing both nitrogen-rich and oxygen-rich functional groups, endows it with remarkable energy content. ADN is a chlorine (Cl)-free oxidizer, producing less harmful and non-toxic products while burning (in comparison to AP), leading to significantly lower environmental impact. AN is another candidate as a chlorine-free oxidizer, but has the disadvantages of a room temperature crystallographic phase transition, hygroscopicity, and a low burning rate [7], leading to lower specific impulse of AN-based solid propellant. Historically, solid propellants have been divided into two categories based on the constituents and their bonding types: homogeneous and heterogeneous forms. A homogeneous physical form characterizes the homogeneous propellants with chemically linked ingredients. Typical homogeneous propellants are single-base (nitrocellouse (NC) and additives), double-base (NC, nitroglycerin (NG), and additives), and triple-base (NC, NG, nitroguanidine, (NQ), and additives). On the other hand, the ingredients in heterogeneous or composite solid propellants are physically mixed. Heterogeneous propellants are usually composed of oxidizers, particles with a crystal-like appearance, embedded into a polymeric fuel binder, and other additives, which forms a highly combustible energetic mixture. Oxidizers like AP, AN, ADN, RDX, and HMX are frequently used [8]. ADN-based propellant brings together the advantages of both composite and monopropellant systems. It offers the high thrust and efficiency of composite propellants while retaining the controllability and versatility of monopropellants. Along with ADN's advantages of a high heat of formation, higher gas yield, lower environmental impact, higher burn rate, and higher specific impulse, there are several challenges to address before its application in solid propellants, such as its high manufacturing cost, hygroscopic nature, low thermal stability, and high sensitivity to mechanical impact [9]. Various techniques [10] have been explored to change the hygroscopic nature and reduce the mechanical and thermal sensitivities of ADN, such as changing its physical structure (by prilling technology), surface coating, and co-crystallization [11]. Among them, polymer-based surface coatings on ADN's surface and co-crystallization are currently emerging techniques to provide high anti-hygroscopic behaviour for ADN composite propellants as well as lower sensitivity to mechanical impacts and greater thermal stability, with the aim of minimizing the risk of accidental ignition during handling, transport, and storage. The lower environmental and health impacts compared to other traditional solid propellants, and technological progress in overcoming the major drawbacks of ADN (sensitivity and hygroscopic nature), make it a valuable choice as a non-carcinogenic [12] "green" solid propellant, replacing the toxic and corrosive AP. Another primary reason for ADN's growing popularity lies in its high oxygen balance (25.8%; higher in comparison to other green alternatives, but lower than the 34.04% of AP) and its energetic performance. The dinitraminic and nitraminic functional groups present in ADN contribute significantly to its energy content due to a higher heat of formation in comparison to AP. The high heat release enables the formulation of ADN-based propellants with enhanced specific impulse and combustion efficiency. The lower density with higher specific impulse of ADN, as

compared to AP, can also lead to an overall mass reduction of the propellant and increased payload for a given launch vehicle.

Ammonium dinitramide is chemically denoted as $NH_4N(NO_2)_2$ or ADN. It is a white crystalline solid, generally synthesized by reacting urea with nitric acid. ADN's structure contains both ammonium cations (NH_4^+) and dinitramide anions ($N(NO_2)_2^-$). The dinitramide anion consists of two nitro groups (NO_2) connected to a central nitrogen atom, which gives ADN a relatively high oxygen content (in comparison to AN), making it an efficient oxidizer. The dinitramide anion imparts energetic properties to ADN, making it suitable for use in propellants and explosives [13]. Furthermore, researchers have investigated various ADN-based formulations by combining them with energetic binders, plasticizers, and metal additives to enhance its performance and develop alternatives to traditional composite solid propellants based on AP. The ignition and combustion of metal fuels within a propellant matrix is a process characterized by its exothermic nature, yielding substantial energy upon initiation. ADN's oxygen-rich molecular structure and high heat of formation leads to an environment conducive to the controlled oxidation of metal particles, ensuring optimal energy release and controlled combustion kinetics. The availability of sufficient oxygen atoms for metal fuel oxidation addresses the challenges of incomplete combustion and potential overheating, leading to overall enhanced propellant stability and performance. These efforts have led to the development of ADN-based propellants with superior specific impulse, combustion efficiency, and thrust characteristics [14–16]. The use of ADN is not limited to traditional space propulsion and military applications; it has also garnered attention in emerging fields such as in-space propulsion and small-scale launch systems. The energy density of ADN-based propellants offers advantages for miniaturized propulsion systems, enabling cost-effective and efficient satellite manoeuvres [17] using the ADN-based liquid propellant LMP-103S [18]. Further, to increase the applicability of ADN in both solid and liquid propulsion systems, detailed studies using theoretical, computational, and experimental approaches should be utilized in the future to overcome the challenges associated with the development of ADN-based green propellants. This review is focused on the combustion behaviour of ADN-based composite solid propellant with metallic fuels. The combustion of composite solid propellant is a complex research problem: the overall performance highly depends on melting, sublimation, thermal decomposition, ignition, and burning of all the ingredients, as well as mutual interactions of different reaction products and their impact on the flame structure in spatial and temporal zones. Hence, this review paper explores previous research conducted on ADN and various ADN-based compositions from the energetic performance point of view. The review paper systematically constructs a discussion on the physiochemical properties of ADN, thermal decomposition pathways of ADN, ADN's combustion characteristics and their dependence on various operating parameters, and later, combustion studies on ADN-based composite solid propellants with metallic fuels. In the last section, various research pathways are identified to enable sustained efforts for future development of ADN-based green solid propellants to replace traditional toxic, polluting propellants currently used for space propulsion.

2. Physiochemical Properties of ADN

ADN is normally found as white crystalline particles that are solid. Depending on the manufacturing and processing steps used to produce ADN, these particles can have different sizes, from tiny granules to large crystals. ADN's white appearance is caused by light dispersion by its crystal lattice. The attributes and behaviours of ADN are strongly influenced by its orthorhombic crystalline structure, which implies that all its atoms are set up in a lattice having orthogonal (90°) positions with their crystallographic axes in

three dimensions. The stability and reactivity of ADN can be modified by considering the arrangement of various elements in its crystalline structure through different synthesis and processing methods. ADN can be employed in its larger crystal shape for certain purposes or shredded into smaller particles to improve its responsiveness and combustible properties. ADN's crystalline structure and physical form must be considered when formulating propellants and explosives because they have an impact on its performance properties like burn rate, sensitivity, and overall performance [19].

Table 1 describes the physiochemical properties of various oxidizers along with ADN. The dinitramide anion ($N(NO_2)_2^-$) with the ammonia cation (NH_4^+) combines to form the granular white compound ADN with an excellent oxygen balance (OB) of around 25.8%, higher than AN but lower than AP. It has higher heat of formation (−148 kJ/mol) and lower density in solid state (1.81 g/cm^3) compared to AP (1.95 g/cm^3). The molar volume and associated density within the liquid phase at 25.0 °C are 74.08 cm^3/mol and 1.675 g/cm^3 [20], respectively.

Table 1. Physiochemical properties of various oxidizers; reproduced/adapted from [21] under license CC BY-NC-ND 4.0 by Elsevier.

Parameter	AP	ADN	AN	RDX	HMX	Cl-20	HNF
Formula	NH_4ClO_4	$H_4N_4O_4$	$H_4N_2O_3$	$C_3H_6N_6O_6$	$C_4H_8O_8N_8$	$C_6H_6N_{12}O_{12}$	$N_2H_5C(NO_2)_3$
Density (g/cm^3)	1.95 [22]	1.81 [23]	1.72	1.81	1.91 [22]	2.04	1.82 [24]
Molecular weight	117.49	124.07	80.04	222.12	296.2	438	183.03
Oxygen balance (%)	+34.04	+25.8	+19.98	−21.61	−21.61	−10.96	+13.11
ΔH_f (kJ/Mol.)	−290.45 [22]	−148 [23]	−369.00 [25]	+61.53	+74.89 [22]	+415.47 [26]	−72 [26]
T_{onset} [a] (°C)	308.06 [27]	150 [28]	272.73 [29]	209.20 [27]	280.56 [27]	-	-
T_{exo} [b] (°C)	354.02 [27]	190 [28]	-	241.56 [27]	285 [27]	226.85 [30]	133 [31]
Melting point (°C)	>300	91–93 [32]	169.6	203.85 [25]	282.1 [33]	- [c]	131.17 [31]

[a] Refers to the decomposition temperature of the oxidizer. [b] Refers to the exothermic peak temperature of the oxidizer. [c] Cl-20 decomposes before melting.

The melting point of pure ADN is reported as 91–93 °C, which is lower than AN and AP, while ADN decomposes completely at 200 °C. It possesses an endothermic melting peak between 91 °C and 93 °C, subsequently undergoing exothermic disintegration between 150 °C and 210 °C. In addition to that, one endothermic breakdown of ammonium nitrate (AN) in situ. As discussed in the previous section, the main challenges for replacing AP with ADN are its hygroscopic nature and impact sensitivity. A mass of 357 g of ADN can dissolve in 100 g of water at 20 °C [20]. It also has higher solubility in polar solutions but lower solubility in non-polar substances. ADN is a chlorine-free solid propellant, leading to a lower environmental impact when used as an oxidizer in a composite solid propellant; it is also considered as non-carcinogenic and non-allergenic based on toxicological tests [34]. It does not cause irritation to the skin or eyes; however, it can cause irritation if inhaled or swallowed. These positive characteristics of ADN make it an excellent choice of oxidizer for developing a composite green solid propellant with a low environmental impact. Due to its non-toxicity and lower health hazards, ADN-based solid propellants can also have lower environmental impact during manufacturing, handling, storage, and operations; however, future research should address the challenges of its hygroscopicity and thermal and mechanical sensitivities.

3. Thermal Decomposition of ADN

The primary methods used for the understanding of the thermal decomposition of ADN include reaction pathway analysis by identifying its breakdown processes and reaction products using kinetic evaluation and theoretical modelling based on various experimental observations. Several variables, including the pressure, temperature, isothermal as well as non-isothermal boundary conditions, the magnitude of the chemical reaction, catalytic processes, and the type of species formation, can impact the thermal decomposition of ADN. ADN has a lower melting temperature than AN and AP; it starts melting at 91–94 (°C) and it decomposes very rapidly into AN and its by-products above 150 °C due to its higher heat of formation (in comparison to AN and AP). Experimental research on the thermal decomposition of ADN has been conducted by many researchers and various pathways have been suggested depending on the pressure, temperature, and experimental methods employed. Rossi et al. [35] studied the thermal decomposition of ADN inside a vacuum chamber, coupled with thermal analysis techniques (such as quadrupole mass spectrometer TG-QMS for residue gases and Fourier transform infrared spectroscopy (FTIR) for the condensed state). The following possible thermal decomposition pathways were suggested:

$$NH_4N(NO_2)_2 \longrightarrow NH_3 + HN(NO_2)_2 \longrightarrow NH_3 + HNO_3 + N_2O$$
$$NH_4N(NO_2)_2 \longrightarrow 2\,NH_2NO_2 \longrightarrow 2\,N_2O + 2\,H_2O$$
$$NH_4N(NO_2)_2 \longrightarrow NH_4NO_3 + N_2O$$

Under vacuum experimental conditions with low heating rates, ADN decomposition starts with formation of ammonia (NH_3) and dinitraminic acid (HDN or $HN(NO_2)_2$). At 169 °C, major decomposition products observed include HDN, NH_3, nitrous oxide (N_2O), nitric oxide (NO), and water (H_2O). The absence of nitric acid (HNO_3) and the formation of NO and H_2O were attributed to heterogeneous decomposition of (HNO_3) on the chamber wall. The intermediates ammonium nitrate (NH_4NO_3) and nitramide (NH_2NO_2) were not observed under these experimental conditions. The formation of ammonia, nitric acid, and nitrous oxide are important identifiers as they contribute to the overall chemical reactions and subsequent steps in the thermal decomposition of the ADN propellant. Further, Brill et al. [36] investigated the thermal decomposition behaviour of ammonium nitrate (AN), as well as ADN, during rapid pyrolysis at high temperatures close to a burning surface by employing T-jump/Fourier transform infrared (FTIR) spectroscopy. In contrast to AN, ADN shows rapid decomposition, with strong exothermic heat release and formation of NH_3, HNO_3, and N_2O in the early decomposition process at atmospheric pressure (1 atm) and above. It was also found that the condensed part of AN decomposes in a net endothermic manner until a pressure of 33 atm. The thermal and spectral characteristics are in accordance with the reaction of NH_3 with NO_2 serving as the primary source of exothermic heating for the decomposition of AN above 33 atm and ADN at 1 atm and higher pressures. Following this, Oxley et al. [37] investigated the thermal decomposition of ADN and its precursor potassium dinitramide (KDN) in pure form as well as their aqueous solutions. First-order kinetics (in the temperature range 160–210 °C) leads to more than 50% decomposition of ADN, with a free-radical decomposition mode above 160 °C and an ionic decomposition mode below 160 °C, affected by acidity. Differential scanning calorimetry (DSC) traces with a heating amount of 20 °C/min, revealed that the ADN decomposition process shows two endothermic peaks at 94 °C and 301 °C and two exothermic peaks at 189 °C and 274 °C. The first endothermic peak is related to ADN melting, while the highest exothermic peak at 189 °C is related to ADN decomposition into nitrous oxide and nitrate (or nitric acid). The second exothermic peak at 274 °C is related

to further decomposition of AN formed during the first exothermic peak, while the second endothermic peak at 301 °C is related to the formation and vaporization of water during AN decomposition. KDN, a precursor of ADN, on the other hand, is found to be more stable, with a decomposition process similar to ADN, but with one exothermic (239 °C) and two endothermic (130 °C and 274 °C) peaks. Further, Lobbecke et al. [38] implemented various thermo-analytical approaches to study the thermal decomposition characteristics of ADN at isothermal conditions as well as linear heating rates of 0.5–10 K/min. The major products of ADN's decomposition were found to be NH_4NO_3, NH_3, $HN(NO_2)_2$, etc. ADN starts melting at 91 °C and it starts to break down into NH_3 and dinitraminic acid (HDN) at 127 °C. Following HDN's formation, HDN decomposes exothermally immediately into N_2O and nitric acid HNO_3. Nitric acid and ammonia recombine to form AN intermediately, which decomposes at higher temperatures. In the first process (ADN to AN and N_2O), the mass is reduced by 30%; in the second step (converting ADN into gaseous products), the bulk mass is reduced by 70%. ADN splits into N_2O and water at elevated temperatures. Evolved gas analysis was used to identify the drop in AN at temperatures higher than 200 °C with the rise in nitrogen dioxide in a second evaporation phase. For ADN's prospective application as an energetic material, the author provides a thorough explanation along with the key reactions of its thermal characteristics and breakdown behaviour, as below:

$$\begin{aligned} NH_4N(NO_2)_2 &\longrightarrow NH_3 + HN(NO_2)_2 \\ &\longrightarrow NH_3 + HNO_3 + N_2O \\ &\longrightarrow NH_4NO_3 + N_2O \\ NH_4N(NO_2)_2 &\longrightarrow N_2O + 2\,H_2O \end{aligned}$$

Along with the main reactions above, the authors [38] also suggested side reactions for the formation of an additional amount of NO_2, NO, N_2, and O_2, detected using FTIR and mass spectrometry, as follows:

$$\begin{aligned} HN(NO_2)_2 &\longrightarrow N_2O + NO + 0.5\,H_2O + 0.75\,O_2 \\ &\longrightarrow 1.5\,NO_2 + 0.5\,NO + 0.5\,N_2 + 0.5\,H_2O \\ HNO_3 &\longrightarrow NO + 0.75\,O_2 + 0.5\,H_2O \\ &\longrightarrow NO_2 + 0.5\,H_2O + 0.25\,O_2 \\ 2\,NH_3 + 2\,NO_2 &\longrightarrow NH_4NO_3 + N_2 + H_2O \\ &\longrightarrow N_2O + 3\,H_2O + N_2 \\ &\longrightarrow NO + 1.5\,N_2 + 3\,H_2O \end{aligned}$$

$$\begin{aligned} 2\,NH_3 + 3\,N_2O &\longrightarrow 3\,H_2O + 4\,N_2 \\ 2\,NO_2 + H_2O &\longrightarrow HNO_3 + HNO_2 \end{aligned}$$

Vyazovkin et al. [39] employed temperature-controlled gas cell and thin-film laser pyrolysis techniques to study the thermal decomposition of ADN at moderate (in range of 20–250 °C) and high temperatures (up to 630 °C). The study suggested that the ADN decomposition mechanism involves N_2O and NO_2 as primary products in both temperature ranges, followed by NO formation in the later stages of the reactions. N_2O, NO_2, NO, NH_3, and HNO_3 were the main gaseous products of ADN decomposition that were discovered in the gas cell studies with continuous heating regimes of 1.5 °C/min–20 °C/min. The gas products were tracked using FTIR at assigned absorption bands and intensities were converted to relative concentrations in the gas cell experiment. NO_2 was observed at temperatures as low as 50 °C, followed by detection of HNO_3. NO and NH_3 were observed beyond 100 °C. In laser pyrolysis experiments, with high heating rates, along with N_2O and NO_2 formation and NO detection in the later stages, there was no detection of NH_3. This is evidence for direct decomposition of ADN without forming AN when subjected to high heating rates. The authors suggested that the obtained mechanism of ADN decomposition could be utilized for further combustion modelling of ADN. Fetherolf et al. [40] experimentally distinguished CO_2 laser-induced pyrolysis (LIP) and laser-induced regression (LIR) of ADN pellets in an argon atmosphere in the pressure range of 0.3 to 1.0 atm and incident heat flux rates of 20 to 300 W/cm^2, along with laser-induced combustion at higher pressures. Under the LIP testing at 0.1 and 0.3 atm with an incident heat flux of 20 and 30 W/cm^2, the specimens gradually melted, creating a melt layer, which boiled, as large gas bubbles formed and evolved from the melt layer. The decomposition of ADN follows two mechanisms: (1) Slow pyrolysis, producing N_2O and H_2O along with AN particles; and (2) rapid pyrolysis, leading to higher production of NO_2 and NH_3, along with small amounts of N_2 and NO. The temporal evolution shows that slow pyrolysis is dominant at 0.1 atm with 20 W/cm^2 heat up to 2100 ms, while onset of rapid pyrolysis occurs beyond 2100 ms. The test at 0.3 atm with 30 W/cm^2 shows only the rapid pyrolysis decomposition pathway, occurring after 275 ms. At and above atmospheric pressure, with a heat flux between 50 and 300 W/cm^2, due to laser-induced regression, stable regression of the melt layer without a luminous flame was observed. At atmospheric pressure and a lower heat flux (50 W/cm^2), the melt layer's thickness grew extensively, turning to a brownish-white colour (NO_2 from HNO_3 decomposition) and then abruptly erupted and dissipated with rapid pyrolysis, producing a dense cloud of AN particles as a smokey plume. In LIP testing quasi-steady regression was not observed at sub-atmospheric pressure, while in LIR testing, steady regression along with higher N_2 evolution was observed, with a significant fraction of AN particles. The results of element balance in LIR suggested a higher amount of AN formation compared to Brill et al. [36], which was attributed to differences in the experimental conditions. The regression rate did not change significantly with an increase in laser heating, suggesting that sufficient heat was available in the gas phase close to the surface during LIR testing. Park et al. [41] used pyrolysis/mass spectrometry to assess the outcomes of the thermal decomposition of ADN in a gaseous state under low pressure, and temperature conditions of 373–920 K. In order to predict the production rates of NH_3, H_2O, N_2, and N_2O, ab initio molecular orbital and canonical variational Rice–Ramsperger–Kassel–Marcus (MO/cVRRKM) algorithms were used. The researchers discovered and observed the unimolecular breakdown of dinitraminic acid (HDN), $HN(NO_2)_2 \longrightarrow HNNO_2 + NO_2$, followed by the rapid decomposition reaction $HNNO_2 + M \longrightarrow N_2O + OH + M$, which triggered the reaction of the sublimed ADN as the combination of NH_3 and $HN(NO_2)_2$. The study obtained the rate constants of key reactions using theoretical modelling (MO/cVRRKM algorithm) and validation with measured

quantities of NH_3, H_2O, N_2, and N_2O at 10 Torr, using calibrated reference mixes. The suggested key reactions are listed below: Chain initiation reactions:

$$HN(NO_2)_2 \longrightarrow HNNO_2 + NO_2$$
$$HNNO_2 + M \longrightarrow OH + N_2O + M$$

Chain propagation reactions:

$$OH + NH_3 \longrightarrow H_2O + NH_2$$
$$NH_2 + NO_2 \longrightarrow H_2NO + NO$$
$$NH_2 + NO \longrightarrow H + N_2 + OH$$

The researchers hypothesized that at elevated pressure settings, subsequent radical–radical interactions featuring $HNNO_2$ would become more relevant due to the rising radical species levels.

$$\begin{aligned} HNNO_2 + OH &\longrightarrow HNOH + NO \\ &\longrightarrow HNO + HONO \\ HNNO_2 + NO &\longrightarrow HNNO + NO_2 \\ &\longrightarrow HONO + N_2O \\ HNNO_2 + NO_2 &\longrightarrow HNO + N_2O_3\,(NO + NO_2) \\ &\longrightarrow HNO_3 + N_2O \end{aligned}$$

Correspondingly, Ermolin et al. [42] examined the decomposition of ADN sublimation products at low pressure (10 torrs) in the temperature range of 373 K–920 K by using numerical simulations. The study describes two previously suggested pathways for ADN sublimation: (1) Direct evaporation to vapour and (2) dissociative sublimation to NH_3 and dinitraminic acid. The numerical simulation was performed for the pyrolysis process using a one-dimensional reactor. A comparison with the experimental data of [41] suggested the dissociation pathway of ADN sublimation. Further, based on the contribution of various reactions and pyrolysis products at the exit of the reactor (H_2O, N_2O, N_2, NH_3), the rate constants were evaluated for two reactions involved in $HNNO_2$ consumption at lower temperatures and a third reaction related to high-temperature consumption of HNNO. The dissociation reaction that governs the ADN sublimation process can be given as follows (where ADN_c denotes ADN in the condensed phase):

$$ADN_c \longrightarrow NH_3 + HN(NO_2)_2$$

A two-stage ADN thermal decomposition mechanism was proposed by experimentally using a two-temperature flow reactor at 800 Pa (Shmakov et al. [43]). The ADN vapour pressure at temperatures between 80 °C and 140 °C was obtained and the heat of vaporization was calculated, which confirmed that ADN thermal decomposition involves vaporization before being dissociated into NH_3 and $HN(NO_2)_2$. The effective rate constants of ADN vapour dissociation at temperatures between 160 °C and 320 °C were determined by measuring the mass of the condensed substance at the exit from the second stage of the flow reactor. At 800 Pa, the degrees of ADN breakdown (α) along with the effective decomposition rate characteristic (k_{eff}, s^{-1}) were obtained as (0, -), (0.1, 3.1), (0.21, 7.8), (0.32, 14.0), and (0.82, 71.8) at temperatures of 140 °C, 160 °C, 200 °C, 240 °C, and 320 °C, respectively. The kinetics of thermal decomposition of ADN vapour was investigated by modelling the gas-phase reaction mechanism (172 reactions) and comparing the experimen-

tal data obtained by a mass spectrometer at the exit of the second reactor, with operating temperatures between 160 °C and 900 °C. The reaction rate constants were evaluated to interpret the experimental data, which could be used in modelling the ADN flame. In accordance with the above, Santhosh et al. [44] studied the change in the activation energy (E_a) with conversion (α) for ADN prills. The isothermal and non-isothermal decomposition kinetics for ADN prills were characterized by employing thermogravimetry analysis (TGA). The differential isoconversional (Friedman, FR) and integral isoconversional (Vyazovkin) approaches were used to establish the dependency between the activation energy and conversion. The outcome suggested that E_a values for the conversion $(0.2 \leq \alpha \leq 0.95)$ fall within the sequence of Vyazovkin > FR (Friedman) > standard isoconversional technique, while the trends between E_a and α across all three technique was similar. The E_a value rises in the early phases of breakdown $(0.05 \leq \alpha \leq 0.2)$ but falls in the final phases of decomposition $(0.2 \leq \alpha \leq 0.95)$. Thermal stability for ADN prills was reported to be significantly greater compared to that of pure solid ADN. The study suggested that ADN prills undergo single-stage decomposition with 100% mass loss at temperatures between 145 and 230 °C for heating rates of 2, 3, 6 °C/min. The generalized decomposition of ADN induces a variety of nitrogen oxides, with the generation of ammonia as well as dinitraminic acid [$HN(NO_2)_2$] dominating in the initial process (temperatures under 100 °C), subsequently followed by an additional breakdown of the latter as well as the formation of AN at elevated temperatures above 100 °C through the recombination of NH_3 and HNO_3. The generalized thermal decomposition of ADN was summarized through the following reactions:
At lower temperatures:

$$NH_4N(NO_2)_2 \longrightarrow NH_3 + HN(NO_2)_2$$
$$HN(NO_2)_2 \longrightarrow HNO_3 + N_2O$$

At elevated temperatures:

$$NH_3 + HNO_3 \longrightarrow NH_4NO_3$$
$$NH_4NO_3 \longrightarrow N_2O + 2\,H_2O$$
$$HN(NO_2)_2 \longrightarrow {NO_2}^+ + {HNNO_2}^-$$

Likewise, the research conducted by Matsunaga et al. [45] used a highly sensitive calorimeter (TAM) for isothermal measurements and a DSC for non-isothermal examination of the exothermal behaviour of the ADN decomposition kinetics. The DSC curve showed two endothermic and two exothermic events, as predicted by previous studies. The two heat generation peaks belong to the reactions shown below, where AN and N_2O are generated during the first event and AN further decomposes into N_2O and water.

$$NH_4N(NO_2)_2 \longrightarrow NH_4NO_3 + N_2O$$
$$NH_4NO_3 \longrightarrow N_2O + 2\,H_2O$$

The study also predicted the lifetime of ADN for storage applications by the non-isothermal DSC method and the TAM isothermal method. It was found to be much longer by the non-isothermal method compared to the isothermal method. It was suggested that non-isothermal DSC analysis is not suitable to accurately predict the lifetime of ADN-like substances, whose decomposition mechanisms vary with the surrounding temperature. The study suggested using isothermal methods to predict the lifetime of ADN at low temperatures. The study also analysed an (11-year-old) aged sample of ADN as well as a new sample and suggested that apart from temperature, other factors of the storage

environment can impact the decomposition of stored samples. Impurities of AN in ADN, which is one of the products of the ageing and thermal decomposition of ADN, can reduce the melting point of ADN significantly. The study also predicted the lifetime of liquid ADN as less than 1 year at a temperature of 55 °C.

In order to distinguish the thermal decomposition pathways of ADN, Andreev et al. [46] synthesized two ADN samples labelled with isotopic nitrogen ^{15}N: one with a label on the NH_4^+ cation and another with the label on the central nitrogen atom of the anion $N(NO_2)_2^-$. The thermal decomposition of the isotopic ADN sample with ^{15}N in the cation, showed the absence of ^{15}N in NO and N_2O, which suggested that the source of these oxides is from decomposition of the anion. However, the ^{15}N label was found in N_2 gas in the form of $^{15}N^{14}N$, which increased from 40% at low conversions to 90% at total ADN decomposition during the experiment. The thermal decomposition of ADN with the ^{15}N label on the central nitrogen atom in the anion resulted in finding labelled ^{15}N in N_2O in the form of $^{15}N^{14}NO$ and partially in N_2 and NO (10% of the total content of gases). The acidic content of the residue (HNO_3) after thermal decomposition was also traced during the experiments. The following (not balanced) reactions reveal the gas-phase pathways of ADN decomposition:

$$^{15}NH_4N(NO_2)_2 \longrightarrow {}^{15}NN + NO + N_2O$$
$$NH_4^{15}N(NO_2)_2 \longrightarrow N_2 + {}^{15}NNO + NO$$

The study concluded that the oxidation of the ammonium cation in ADN decomposition leads to formation of N_2 and an autocatalyst, while acid decomposition of the anion leads to formation of N_2O and NH_4NO_3. This study further explored the use of readily oxidized compounds for stabilization of liquid ADN by elimination of the autocatalysis process. Various amines, amides, ammonium salts, and iodides were used as additives (of 1 mol.% and 1 wt.%) to ADN and their efficiencies were evaluated by measuring the induction period (at 120 °C) and initial decomposition rates. The oxidation of additives in the melt layer and their solubility played an important role in stabilizing liquid ADN, while the study suggested future study on the effects of additives on the solid oxidizer. Following this, Mishra et al. [47], carried out low-temperature thermal decomposition of solid ADN at 60, 70, 80, and 90 °C, and investigated mixes (1–2% by mass) of several potential thermal stabilizers to suppress decomposition at low temperatures. Samples (of 100 mg) of ADN with additives were tested in an infrared (IR) heated gas cell in a temperature-controlled nitrogen environment at atmospheric pressure. The formation of N_2O and AN were detected using FTIR at 1-, 2-, or 4-hour intervals up to 7 days. ADN thermal decomposition was observed as a first-order process to produce N_2O and AN in the temperature range of 60–90 °C. The thermal decomposition of ADN with additives such as potassium dinitramide (KDN), potassium fluoride (KF), polymeric phosphorous compound ($P(C_6H_5)_6$, and perhydro-1,3,5-triazine-2,4,6-trione, known as Verkade's super base (VC) were investigated at a constant temperature of 90 °C. It was found that only the KF and VC additives resulted in suppressing the formation of AN. A small amount of AN was observed with KF addition, while no AN was observed with VC. N_2O was observed with all additives, while VC reduced the production rate of N_2O. The results of their studies suggested that Verkade's super base is the best (among those tested) low-temperature stabilizer for ADN.

Many studies which employed differential scanning calorimetry (DSC) for ADN decomposition obtained a total of four spikes in the heat release curve and explained the general thermal decomposition process of ADN [1,36,45–50]. Among these four spikes, two spikes are responsible for the endothermic heat absorption and two for the exothermic

heat release. At 91 °C–95 °C, the first endothermic spike occurs as ADN starts to melt. Following this, the first high exothermic spike occurs at a temperature range of 150 °C–190 °C, forming ammonium nitrate (AN) and N_2O, releasing a high amount of energy. There are two pathways that have been suggested for AN formation: first, direct decomposition of ADN into AN and N_2O; and in the second pathway, ADN first decomposes into NH_3 and HDN, and HDN further decomposes to N_2O and HNO_3. At elevated temperatures, under an acid catalysis reaction, HNO_3 and NH_3 combine and form ammonium nitrate (AN), releasing a high amount of energy. Further, the produced ammonium nitrate starts to break down into N_2O and water, releasing energy, and this becomes the reason for the second smaller exothermic spike, which was observed at temperature of 274 °C. While AN is dissociating, it allows the generation and vaporization of H_2O, which leads to the second small endothermic spike at 300 °C. The previous studies have also highlighted the self-accelerated acid-catalytic behaviour of thermal decomposition of ADN melt. Kazakov et al. [51] investigated the kinetics of heat release during the thermal decomposition of liquid ADN at temperatures of 102.4–138.9 °C. The ADN melt consists of NH_4^+ and $N(NO_2)_2^-$ along with a small amount of NH_3 and dinitraminic acid (HDN). The thermal decomposition of the ADN melt occurs in two stages. In the first stage, the oxidation of the ammonium ion to nitrogen, as the products of the decomposition of dinitramide or its ion, which results in the accumulation of HNO_3, leads to self-accelerated rapid decomposition. This was confirmed by adding a solution of HNO_3 into the ADN melt and examining the decomposition rate, which increased with additional HNO_3. In the second stage, formation of AN due to consumption of HNO_3 leads to a decrease in the self-acceleration process. Solid ADN's stability is significantly affected by the presence of AN and water as impurities. An increase in impurities in AN leads to a decrease in the melting temperature of ADN-AN mixtures. An ADN-AN mixture in the ratio 2:1 can form a eutectic mixture with a melting temperature of approximately 60 °C. Hence, the thermal decomposition rate of solid ADN with AN impurities is affected by the melting mechanism. Manelis [52] has found that the addition of 0–17% (by wt.) AN in the ADN mixture leads to a very high decomposition rate at a temperature of 80 °C, while a molar fraction of 20–30% AN in the ADN-AN mixture leads to the opposite effect by reducing the decomposition rate by 30–40% at temperatures of 106–141 °C [53]. Impurities of 0.3–10% of AN in the ADN-AN mixture does not affect the thermal decomposition rate at temperatures of 150–170 °C. Similarly, Pavlov et al. [53] studied the impact of water on solid ADN thermal decomposition at low temperatures of 60–80 °C. A low amount of water (below 0.5%) in the presence of AN does not affect the thermal decomposition rate as it may exist in the absorbed state without forming the liquid state, while the presence of 1% of water in ADN leads to a 6-fold increase in the thermal decomposition rate at a temperature of 80 °C, which is associated with dissolution of ADN in water. A peculiar phenomenon of "anomalous decomposition" is observed when the water content is less than 0.2%, which relates to a sudden increase in the decomposition rate near the melting point of the ADN-AN eutectic mixture. With decreases in the water content to 0.2, 0.12, 0.08, and 0.07%, the decomposition rate of the ADN-AN eutectic mixture (melting point near 60 °C), shows an increase by 1.4, 80, 900, and 8000 times. The anomalous decomposition phenomenon ceases with the presence of water vapour (at pressure 10 torr).

Corresponding to the above findings, an extensive review was carried out by Yang et al. [28], and it can be concluded that both pressure and temperature conditions, and experimental techniques, have a significant impact on the thermal decomposition mechanism of ADN. The primary features involve a sporadic DSC exothermic peak, enormous volumes of AN and N_2O being produced as a result of solid-phase fragmentation, and a two-phase breakdown mechanism with high and low activation energy values at

temperatures above and below 160 °C, respectively. The condensed-phase disintegration of ADN could be the cause of the reduced activation energy (30 kcal/mole), while the gas-phase breakup of ADN may be the cause of the greater activation energy (40 kcal/mole). Along with that, the initial thermal decomposition temperature of 91–95 °C for ADN was given by Chen et al. [21] in their review. Ermolin et al. [54] and Kumar et al. [32] presented an overview of several previous studies regarding the thermal decomposition of ADN. The researchers cover the physical and chemical features of ADN, and dinitramide and its ions $N(NO_2)_2^-$, which are important in ADN breakdown. The research discusses the multiple pathways of ADN, dinitramide, and $N(NO_2)_2^-$ breakdown using previously presented laboratory and simulated data [55].

It can be summarized here that ADN's thermal decomposition pathways and rates are significantly affected by the original ADN sample, the presence of AN- or water-based impurities, storage method, temperature and pressure conditions, and experimental techniques utilized by the researchers. In broad terms, there are two stages that contribute to the thermal decomposition of ADN. ADN starts to separate in the initial stage, eventually producing N_2O and NH_4NO_3. NH_4NO_3 is subsequently degraded in the following phase to yield N_2O and H_2O. Overall, NH_3, HNO_3, N_2O, H_2O, NO, $HN(NO_2)_2$, HNO_3, and N_2 constitute the main decomposition components. The utilization of ADN-based composite solid propellant with metal additives will require characterizing the effects of metals and other additives on the thermal decomposition of ADN not only for its performance estimation during combustion, but also during the preparation, fabrication, storage, transport, and handling operations.

4. Combustion of ADN

Propellants are high-energy materials that burn slowly in a more controlled manner than explosives. The deflagration of solid propellant causes burning from the surface inward and the surface is observed to regress normal to itself at a definite rate, which can be termed the burn rate (or burning rate); it depends on the surrounding pressure, temperature, and composition of the propellant. The burn rate is one of the main parameters that plays a significant role in estimating the efficiency and selection of propellants. The simple relationship between a propellant's burn-rate and pressure can be defined in exponential form (known as Vielle's law) as $r_b = aP_c^n$, where r_b is the burning rate, P_c is chamber pressure, and "a" and "n" are empirical coefficients, which are obtained experimentally for a specific propellant. Composite solid propellants consist of a fuel, oxidizer, and binder (the binder can be an inert or energetic material). The oxidizer is present as filler in a fuel and binder matrix. ADN presents itself as an alternative oxidizer to AP, with higher burn-rate characteristics and chlorine-free combustion products. The combustion characteristics of the oxidizer plays an important role in the efficient performance of composite solid propellants and can be estimated by a variety of theoretical thermochemical calculations, numerical methods, and experimental techniques. Combustion of the ADN exhibits large heat release in the condensed phase, weak thermal feedback with the gas phase, and a low burning surface temperature, resulting in N_2, O_2, and water as combustion products. Additionally, it has a good oxygen balance to secure oxidation of the additive metallic fuel and energetic binder when combined as a composite propellant. The burn rate of ADN as a monopropellant is found to be higher than many highly energetic materials such as AP, AN, HNF, HMX, Cl-20, and glycidyl azide polymer (GAP) at 68 atm [56]. The calculated flame temperature of ADN was found as 2035 K, which remains lower than HNF, HMX, and Cl-20, while it is higher than AN, AP, and GAP. In a composite propellant of ADN with an HTPB (hydroxyl-terminated butadiene polymer) binder, the calculated flame temperature above the surface was found to be closer to the composite propellant of AP/HTPB. Another

important factor in selecting the oxidizer is the particle size or oxidizer dispersity. In comparison to AP, the burn rate of ADN increases with an increase in particle size, while it decreases for AP [57]. The combustion mechanism of the individual oxidizer impacts the selection and the required fabrication steps to prepare the composite solid propellant. Hence, it is important to understand the combustion mechanism and involved processes to integrate the ADN oxidizer with the fuel, binder, and other additives. ADN combustion can be characterized by fast reactions in the condensed phase and slow reactions in the gas phase. Merzhanov et al. [58] studied two types of elementary condensed-phase combustion models. The first model suggests that the combustion is regulated by the total substance conversion in the combustion wave, where the velocity of wave propagation is governed by the maximum flame temperature (T_{max}). The second model suggests the development of the combustion interface as a result of physiochemical reactions (such as evaporation, sublimation, and dispersion), where the burn rate and material conversion are dependent on the surface temperature (T_s) and the depth of reactions (h). The energetic materials exhibit flameless combustion characteristics at low pressure, and with further increases in pressure a high-temperature flame occurs. The combustion of volatile energetic materials is generally described by the second type of condensed-phase combustion model, where a condensed substance produces a large amount of gases, dependent on the physiochemical route, governed by the available heat flux from the gas phase to the condensed phase, and combustion occurs in stages. The interface temperature and kinetics of the condensed-phase reactions are the most significant variables in the condensed-phase combustion model.

Initial experimental studies related to ADN combustion focused on estimating the burn rate and identifying its dependencies as well as characterizing the flame structure, i.e., the spatial distribution of temperature and species in the ADN flame, which led to the development of computational models as well as chemical kinetics for the same. Atwood et al. [59,60] measured the burn rate of many energetic materials (AP, ADN, RDX, HMX) at various pressures and initial temperatures and their sensitivity to initial temperature. At room temperature, the burn rate of ADN was measured over a pressure range of 0.69–10.34 MPa and at two initial temperatures of 298 K and 348 K. The burn rate of ADN was found to be the highest (19.86–36.91 mm/s) among the energetic materials, including AP (2.64–11.5 mm/s). The higher initial temperature of ADN further led to increased burn rates. Korobeinichev et al. [61,62] employed probing mass spectrometry to deflagration flames of ADN pellets between the pressures of 1 and 6 atm. A self-sustaining ADN flame was observed at 6 atm pressure with a burn rate of 19 mm/s and burning temperature of 1080 °C, while flameless combustion was observed at 1 and 3 atm, with burn rates of 3.44 and 12 mm/s, respectively. At 1 and 3 atm, the main reaction products were found to be NH_3, NO, NO_2, N_2O, H_2O, HNO_3, and N_2. With an increase in pressure (at 3 atm), the amount of NH_3 and HNO_3 decreased. The temperatures near the burning surface for 1 atm and 3 atm were measured as 320–350 °C and 550 °C, respectively, along with the presence of AN at lower pressure. The species and temperature profiles were obtained for a high-pressure ADN flame 2 mm away from the burning surface. Strunin et al. [63] suggested that the mechanism of ADN combustion is similar to other onium salts and measured the burn rate and its dependencies on pressure and different additives. It was found that ADN burns without a luminous flame below 0.1 MPa and with a luminous flame above 0.1 MPa. The measured burn rates at 66 kPa, 0.1 MPa, 2 MPa, and 6 MPa were 2.2 mm/s, 2.7 mm/s, 18.2, and 22.6 mm/s, respectively. The burn rate for a 5 mm sample tube of ADN was found to be significantly slower than for a 7 mm sample tube at pressure below 3.0 MPa. The temperature profiles were obtained for pressures of 66 kPa to 6 MPa. In the low-pressure environment at 66 kPa, a small temperature rise occurred across the burning surface, while in the high-pressure environment of 2 MPa, the high-temperature flame was lifted above

the surface by a "dark zone", with a surface temperature of 700 K and flame temperature of 2640 K due to high condensed-phase decomposition. Zenin et al. [64] obtained the thermal structure of an ADN flame in a nitrogen environment for a pressure range of 1–80 atm and temperatures of −150 °C, 20 °C, and 80 °C. In a low-pressure environment (<40 atm), irregular pulsation in the gas-phase temperature measurements were observed for all cases. At elevated pressures, for all sample temperatures, stable ADN combustion with smooth temperature variations was observed. The significant heat release in the solid phase (under or on the burning surface) governs the burn rate of ADN combustion. The authors suggested that the high-temperature flame region could not influence the burn rate of ADN due to low heat feedback from the gas phase to the solid phase. For operating temperatures near to ADN's melting point (+80 °C case), accelerated burning took place.

In order to understand key physical and chemical process involved in ADN combustion, Fetherolf et al. [40] experimentally studied CO_2 laser-induced combustion of ADN pellets in an argon atmosphere above 3 atm and incident heat flux rates of 20 to 300 W/cm^2. The quantitative spatial and temporal profiles of gas species were measured by microprobe/mass spectrometer, and the gas-phase temperature profiles and surface temperatures were measured by using fine-wire thermocouples. The three distinct combustion regimes were identified as laser-induced pyrolysis (LIP) at sub-atmospheric pressure, laser-induced regression (LIR) at atmospheric pressure and above, and laser-assisted combustion (LAC) beyond 3 atm. At ambient pressure, no luminous flames were observed, expect in the high-heat-flux testing case, where sporadic flames were observed. A quasi-steady luminous flame was observed at 3 and 5 atm pressure. The onset of the flame was observed with the beginning of rapid pyrolysis (vigorous gas evolution) or shortly after it. The regression rate at 3 atm and 100 W/cm^2 was 11 mm/s, which increased to 20–25 mm/s at 5 atm. The stand-off distance of the luminous flame from the surface was between 0.6 mm and 1.5 mm. The temperature profile identified a primary reaction zone within/near the surface, followed by a "preparation zone", where the temperature of the gas slowly rose, before high-temperature measurements in the luminous flame zone. At 3 atm and 100 W/cm^2, the observed surface temperature rose to approximately 365 K, with the gas-phase temperature in the "preparation zone" reaching 740–780 K, and a flame temperature of 1250–1330 K. Flamelets were visible close to the surface and the flame structure was substantially different at 5 atm. The surface temperature was 670 K, the gas-phase temperature was 830 K, and the flame temperature was 1400 K. The flame reactions consumed NH_3, NO_2, and N_2O and produced significant quantities of NO and H_2O and very little N_2. The reactions, however, did not reach equilibrium products. Ermolin [65] conducted a numerical study of the ADN flame structure based on the experimental data of [41,64,66] and the decomposition mechanism from [42,48,50,67]. The study investigated the contribution of HDN, aerosols, and ADN vapour in heat release in the flame region surrounding the burning surface in the pressure range of 0.4–60 atm. They hypothesized that HDN entering via the dissociative evaporation pathway of ADN was the primary cause of heat transfer in the cool flame region at $p \geq 3$ atm. The primary flame region next to the burning surface is caused by heat release due to dinitraminic acid formation. The reaction in the $NH_3/N_2O/NO/NO_2/HNO_2/HNO_3$ mixture causes heat release in the high-temperature flame zone, also known as the second high-temperature flame region. The induction zone, which separates the high- and low-temperature regions at intermediate pressures, generates OH radicals, which are consumed significantly at temperatures above 1000 K. The additional generation of OH radicals leads to a drastic increase in the temperature and formation of this high-temperature flame zone. The stand-off distance variation between the high-temperature flame region and the burning surface at low and moderate pressures is explained by small temperature fluctuations within the induction

region due to the presence of admixtures in ADN and by heat exchange between reacting gases and the surrounding medium. The third flame region is produced by the final balance outcomes of O_2, H_2O, and N_2 as well as the breakdown of N_2O and NO. Likewise, a dark-zone temperature gradient was reported at T = 600 °C − 1000 °C) over a pressure span of 5–40 atm by Fogelzang et al. [68]. Further, ADN combustion chemistry was developed based on experimental methods, and used by Korobeinichev et al. [62,66,69] to analyse the ADN flame structure and its thermal decomposition kinetics for pressure ranges of 1–6 atm, also at 40 atm. The findings revealed that upon ADN breakdown, gaseous ADN is formed, which is then dissociated into ammonia and dinitraminic acid (HDN). The investigation discovered three combustion zones: (1) at 3 atm, adjacent to the burning surface, a "cool flame" zone of width 1–1.5 mm, with the presence of gaseous ADN, with its decomposition resulting in a temperature rise of 150 K; (2) at 6 atm, within 6–8 mm above the burning surface, a second flame zone with a high temperature, where ammonia oxidation by nitric acid led to a flame temperature of 1400 K, producing H_2O, NO, N_2O, and N_2; and (3) at 40 atm, a second high-temperature zone, exhibiting a peak combustion temperature of 2000 K. For the pressure range of 5–20 atm, the temperature profile of ADN combustion shows the presence of two temperature plateaus, termed "dark zones" [64]. At these pressures ranges, the temperature plateau between 600 and 1000 °C is called the first dark zone and the temperature plateau between 1000 and 1400 °C is termed the second dark zone. The dark zone's temperature increases and width decreases with increases in pressure. At pressures below 40 atm, the final flame temperature remains below the theoretically calculated flame temperature of 1600 °C in the presence of dark zones. With an increase in pressure, the increase in flame temperature along with reduction in the width of the dark zone was confirmed. This phenomenon was attributed to higher heat loss to the surroundings in the presence of the dark zone. At 60 atm pressure, there was no observation of a dark zone and the flame temperature was observed, was close to the theoretical maximum flame temperature of 1800 °C. The following Table 2 provides a summary of the propellant's surface temperatures T_s, dark zone temperatures T_d, as well as final flame temperatures T_f at various pressures.

Table 2. Temperature parameters during combustion of ADN; reproduced/adapted from [28] with permission from Springer Nature.

Parameter	Pressures (atm)									Reference
	1	3	5	6	10	20	30	40	60	
T_f, °C	-	≈1050	1000	-	1200	1400	1580	1700	1800	[64]
	-	-	≈800	-	≈1010	≈1010	-	≈1240	-	[68]
	-	-	-	≈1080	-	-	-	≈ 1700	-	[62]
	-	-	≈1120	-	-	-	-	-	-	[40]
T_s, °C	280	-	340	-	345	355	362	368	370	[64]
	300	≈400	-	-	-	-	-	-	-	[40]
T_d, °C	400	-	700	-	800	950	1050	1200	-	[64]
	450	-	≈545	-	≈580	≈620	-	≈780	-	[68]
	≈370	540	-	-	-	-	-	-	-	[62]
	427	≈550	-	-	-	-	-	-	-	[40]

A thermal initiation investigation by electron beam heating in vacuum was carried out by Ramaswamy et al. [70,71] for a single crystal and prills of ADN, produced by a variety of production processes. The phenomenon of microscopic reaction sites through to full crystal consumption was observed by environmental scanning electron microscopy (ESEM). The study suggested that ADN crystals and prill micro-structures had an effect on controlling the formation of microscopic reaction sites, their growth to form a porous substance, and finally creating a hot spot. The chemical purity of the ADN, the micro-structure, and the

presence of thermal stabilizers can all affect its initiation attributes. The micro-structure of ADN, dependent on various manufacturing processes, should be optimized to further enhance the burn rate or performance of ADN as an oxidizer. Sinditskii et al. [72] have studied the burn-rate characteristics of various ADN configurations: (1) ADN pressed strands in quartz tubes and plexiglass tubes; (2) ADN pellets; (3) thin-pressed plates; and (4) single crystals, along with organic and inorganic additives. The burning rates of pure ADN as well as other configurations were measured at constant pressures of 0.1 to 36 MPa. As observed in previous studies, ADN burned without a luminous flame at low pressures, producing white vapour. With an increase in pressure, small flamelets emanating from local reaction sites were observed, similar to [40]. Above 1–2 MPa, the gas became transparent and a luminous flame appeared. Between 2 and 10 MPa pressure, the scatter data in the ADN burn rate (26–54 mm/s) indicated combustion instabilities. In a general trend, the burn rate of pressed ADN strands increased with pressure up to 5.8 MPa and decreased in the range of 5.8–10 MPa, followed by an increase in the burn rate between 10 and 36 MPa. There was no self-sustainable ADN combustion obtained at atmospheric pressure, even with an initial temperature close to the melting point 80 °C. The molten ADN at a temperature of 100 °C, exhibited complete combustion, with a burning rate of 6.7–9.1 mm/s at atmospheric pressure. ADN crystals on the other hand exhibited an inability to burn in the pressure range 2–10 MPa and revealed lower burning rates at 10–36 MPa compared to ADN strands at similar pressures. The attempts to ignite ADN crystals were not successful in pressure range 2–10 MPa due to cracking in crystals and forming splinters, which led to ceasing the combustion process. Addition of 0.2% paraffin to crystalline ADN led to further reductions in the low-pressure limit of ADN-sustained combustion from 0.2 MPa to 0.02 MPa. Between 0.2 and 2.1 MPa and 15 and 36 MPa, the burning rates of 0.2% paraffin + crystalline ADN coincided with pure ADN. The study also suggested that addition of 0.2% paraffin into ADN pressed strands in a plexiglass tube showed sustainable combustion of ADN at atmospheric pressure, which provides an explanation of various studies exhibiting ADN combustion at atmospheric pressure, suggesting that it could be due to insignificant amounts of organic impurities. ADN burning at sub-atmospheric and atmospheric conditions was characterized by a non-luminous flame as well as the formation of condensed-phase products, mainly an ADN-AN mixture. At atmospheric pressure, paraffin-doped ADN decomposition produced a maximum of 57% AN (by mole). ADN within water at a 90% concentration had a local peak burning rate that was twice as high as that of pure ADN. ADN combustion was governed by exothermic condensed-phase decomposition reactions at lower pressure. Between 1 MPa and 10 MPa, gas-phase reactions started playing a role in ADN combustion and were limited by the energetics of the condensed phase. The principal source of heat in the condensed phase was located far from the molten surface layer, where the molten surface was made up of initial ADN and AN. At critical pressures, heat generation in the condensed phase caused thickening of the reaction layer, resulting in the highest degree of dispersal. Excessive porosity or non-polar admixtures can inhibit massive reaction-layer disturbances, lowering the lower-pressure limit of deflagration and lowering burning rates in the pressure range of 1 to 10 MPa. Sinditskii et al. [73], in continuation of the previous study of [72], experimentally employed tiny tungsten–rhenium thermocouples to obtain temperature profiles in the ADN combustion flame at 0.04 to 10 MPa pressure. According to the findings, burning at low pressures is primarily controlled by the ADN decomposition process in the condensed phase. The findings were supported by condensed-phase modelling in [74]. A three-zone

flame structure was identified and the main chemical reactions were proposed with the following key reactions:

$$\begin{aligned}
NH_4N(NO_2)_2(l) &\longrightarrow NH_4NO_3(l) + N_2O + 33\,\text{kcal/mole} \\
NH_4NO_3(l) &\longrightarrow HNO_3(g) + NH_3(g) \\
NH_4N(NO_2)_2(l) &\longrightarrow HN(NO_2)_2(g) + NH_3(g) \\
NH_4N(NO_2)_2(l) &\rightleftharpoons HN(NO_2)_2(l) + NH_3(l) \\
HN(NO_2)_2\,(l/g) &\longrightarrow NO_2 + HNNO_2 \longrightarrow OH + N_2O \\
NO_2\,/OH + NH_3 &\longrightarrow H_2O, N_2, NO, N_2O
\end{aligned}$$

At low pressures (below 1 MPa), flameless ADN burning is governed by a lack of heat feedback from the gas phase to the condensed phase and formation of condensed AN and gaseous N_2O. In the condensed phase and aerosol zone, two competitive reactions govern the temperature of the surface as well the gas zone: (1) ionic: forming condensed AN and gaseous N_2O; (2) dissociative: forming gaseous/liquid HDN and NH_3. At adequate conditions, AN further forms gaseous NH_3 and HNO_3, while HDN dissociates into OH/NO_2 radicals as well as NO and N_2O. Further oxidation of NH_3 by radicals produced by nitric acid forms the first flame zone; total combustion is completed in the second flame zone. Similarly, the other pathway follows an ionic mechanism and results in the formation of the intermediate ammonium nitrite. The formed AN further decomposes, resulting in the formation of water and nitrogen oxides.

$$\begin{aligned}
NH_4N(NO_2)_2(l) &\longrightarrow NH_4NNO_2(l) + NO_2 \\
&\longrightarrow NH_4NO_2(l) + 2\,NO \\
&\longrightarrow 2\,H_2O + 2\,NO + N_2 + 41\,\text{kcal/mole}
\end{aligned}$$

Figure 1a shows the three zone ADN flame structure as proposed by [73]. ADN's surface temperature corresponds to the dissociation temperature of AN. In the aerosol zone (just above the surface), temperature is controlled by the AN dissociation reaction at the surface of small droplets, followed by dissociation of the remaining ADN droplets. The fast decomposition reaction in the condensed phase forms an aerosol zone above the surface; the ADN combustion mechanism is characterized by a slow gas-phase reaction. The decomposition reaction in the melt layer on the surface governs the flameless combustion at low pressures with no heat feedback from the gas phase. In the middle pressure range (1–10 MPa), the fast energy-limited heat release in the condensed phase has to compete with slow and energy-rich heat release in the gas phase, leading to combustion instabilities. At high pressure, above 10 MPa, the condensed-phase decomposition does not govern the combustion, because of a lack of heat produced in comparison to gas-phase decomposition of HNO_3, forming the first flame zone and with complete heat release in the second flame zone. In their thesis, M.L. Gross [75] developed a coupled condensed- and gas-phase model to investigate the ADN combustion flame using the detailed gas-phase chemical kinetics (31 species and 172 reactions) of Korobeinichev et al. [69]. The model predicts burn rate, temperature, species profiles, and temperature sensitivities for the first zone between 0.2 and 2 MPa. The model also predicts burn rates for all regions, while it was unable to predict ADN's unstable combustion region, dark zone lengths, and temperature sensitivities for pressures above 2 MPa. Hence, a modified condensed-phase reaction mechanism is proposed, as shown in Figure 1b, by suggesting an AN decomposition route within the condensed phase, generating a high condensed-phase heat release. The modified

model can predict temperature and species profiles, while it is unable to match pressure exponents, which would require future investigation.

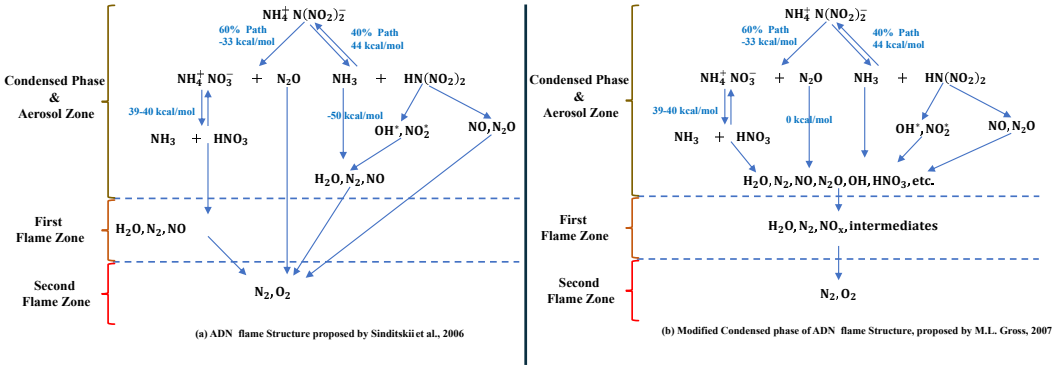

Figure 1. ADN flame structure (**a**) as initially proposed by [73] and (**b**) modified by [75].

Correspondingly, a detailed coupled condensed and gas-phase kinetics model was used by Thakre et al. [76] to construct a framework for the combustion of ADN monopropellant. The conservation equations of mass, energy, and species concentrations for the condensed and gas phases are solved with multiphase modelling. The finite rate chemistry is modelled with three global condensed-phase reactions with 34 species, and 165 reactions of optimized gas-phase chemistry based on [69,77]. A good agreement between predicted [69] and measured temperature and species profiles was obtained. The predicted burn rates were also closely matched with measured burn rates in the range of 0.7 to 350 atm. The ADN burn rate increases with increases in pressure, except in the irregular burning region of the mid-pressure range of 40 to 100 atm. In the low-pressure range (below 20 atm), ADN combustion characteristics of intense heat release in the condensed phase, weak heat feedback from the gas phase, and a high burning rate were captured. In the mid-pressure range, the irregular combustion behaviour was attributed to the competitive effect of condensed-phase and gas-phase reactions, which leads to a reduced burn rate, with a gap in both modes of heat release. At high pressure (above 100 atm), the secondary flame was observed with the primary flame, caused by rapid enhancement in heat feedback from the gas phase to the propellant surface, and gas-phase kinetics governs the ADN combustion process. Figure 2 shows the schematic of the ADN combustion wave structure, representing three segments, solid phase, foam layer, and gas-phase, along with different physical phenomena of forming the melt layer, gasification, aerosol zone formation, and the primary and secondary flame zones. The authors suggested that further improvements in the coupled condensed- and gas-phase ADN combustion model could include: (1) global reactions and kinetics of the condensed phase; (2) gas-phase reactions close to the burning surface; and (3) modelling the heat transfer to predict the final flame temperature at low pressure.

Parr et al. [78] studied laser-induced deflagration of ADN in a sandwich configuration with the energetic binder N-5 double base, where the binder slice (lamina of thickness: 0.5–1 mm) was kept between two rectangular ADN oxidizer pellets (2 mm slab). The combustion of the sandwich forms a diffusion flame, with the flame structure governed by the kinetics of decomposition. The diffusion flame length increases linearly with lamina thickness in the case of the ADN oxidizer and N-5 binder; the dark-zone thickness decreases with increases in pressure (1–15 atm), while the burn rate was found to be independent of lamina thickness and pressure. Korobeinichev et al. [79] experimentally investigated the flame structure of ADN/HTPB composite propellant (with HTPB 3–20% by mass) at pressures of 0.05–0.6 MPa. Non-homogeneous and non-stationary combustion was observed within the flame zone away from the propellant surface in contrast with AP/HTPB

studies. Bright luminous flame jets, with average lifetimes of 0.2 s, emerged from the propellant surface due to agglomeration of melted ADN particles at the burning surface, followed by reaction in a diffusion flame. The reactions in the condensed phase governed the ADN/HTPB combustion. With oxidation, HTPB decomposition products occured in the gas phase, leading to increases in the gas-phase heat release and rapid acceleration of the first and second zones of the ADN flame. Fujisat et al. [80] used a thermoplastic elastomer (TP) and HTPB as binders in composite propellants based on ADN. The study employed the pyrotechnic sensitivity to evaluate the safety of TP/ADN and used a stand burner to estimate the burn rate for various combinations. A theoretical comparison of the specific impulse I_{sp} found that it was higher for ADN-based composite propellant than AP-based composite propellant. The four composite propellants used were TP/ADN-1 (mass ratio 30:70), TP/ADN-2 (mass ratio 20:80), TP/ADN-3 (mass ratio 10:90), and HTPB/ADN (mass ratio 30:70, with prilled ADN), along with TP/AP (mass ratio 20:80) for reference. The linear burn rates for the TP/AP reference sample were observed to be between 3.5 and 5.5 mm/s at the pressure range of 1.1 MPa to 7 MPa, on a log–log scale. The burning of TP/AP showed a melt layer, which could be attributed to TP, as conventional AP combustion does not show a melt layer. All other combinations of composites based on ADN exhibited a steady flame with a melt layer and droplets blown off from the burning surface. The burn rates for TP/ADN-2 (at a similar composition to TP/AP) showed linear burn rates from 3.5 to 24.5 mm/s at a wide range of pressures, from 0.8 MPa to 6 MPa, significantly higher than TP/AP. A comparison between TP/ADN-1 and HTPB/ADN of similar composition showed the HTPB/ADN burn rate was similar to TP/ADN-1 at 3 MPa, while it exhibited a lower pressure exponent of 1.1 compared to TP/ADN-1. TP/ADN-3; with a higher ADN composition showing the highest burn rates of 28 mm/s and 39 mm/s at pressures of 3 and 5 MPa, respectively. The measured final flame temperatures were close to theoretical values for all samples. As a result of the study, it was suggested that a binder's thermal parameters have an impact on its combustion features, and it would be necessary to synthesize binders that are better compatible with ADN. Wingborg et al. [81] formulated a minimum smoke composite propellant based on prilled ADN (coarse: $d_{50} = 200$ μm; and fine: $d_{50} = 60$ μm) and the energetic binder glycidyl azide polymer (GAP). The burn rate measurement for an ADN/GAP (70:30) formulation was found to be 24 mm/s at 7 MPa. The results from a 3 kg rocket motor test firing confirmed the minimum smoke characteristics and high specific impulse of ADN/GAP-based propellant.

To summarize this section, ADN combustion was characterized by various experimental studies related to burn rate measurements, and its dependence on pressure and initial temperature, measuring temperature and species profiles across the condensed and gas phases and aerosol zones as well as in the flame zones. Many experimental studies have observed and characterized the three zones of ADN combustion flames: the condensed and aerosol zone, primary flame, and the secondary flame, with observation of two dark zones. The kinetics of various features of ADN combustion flames have been obtained at various operating pressures and sizes of ADN samples. At low pressures, below 1 MPa, flameless ADN decomposition is governed by condensed-phase reactions and a lack of feedback from the gas phase to the condensed phase; while at medium pressure (1–10 MPa) the condensed-phase and gas-phase energy releases compete with each other, leading to instabilities in the ADN combustion flame; and at high pressures, beyond 10 MPa, stable combustion governed by gas-phase reactions leads to production of the visible first and second high-temperature flame zones. The impact of ADN's physical characteristics (purity, micro-structure, and presence of thermal stabilizers) were also analysed by various experimental studies, along with the impact of the presence of a binder material with ADN. Various computational methods have also been developed to understand and estimate the

burn rates and ADN's flame characteristics, with detailed gas-phase chemistry as well as coupled condensed- and gas-phase modelling.

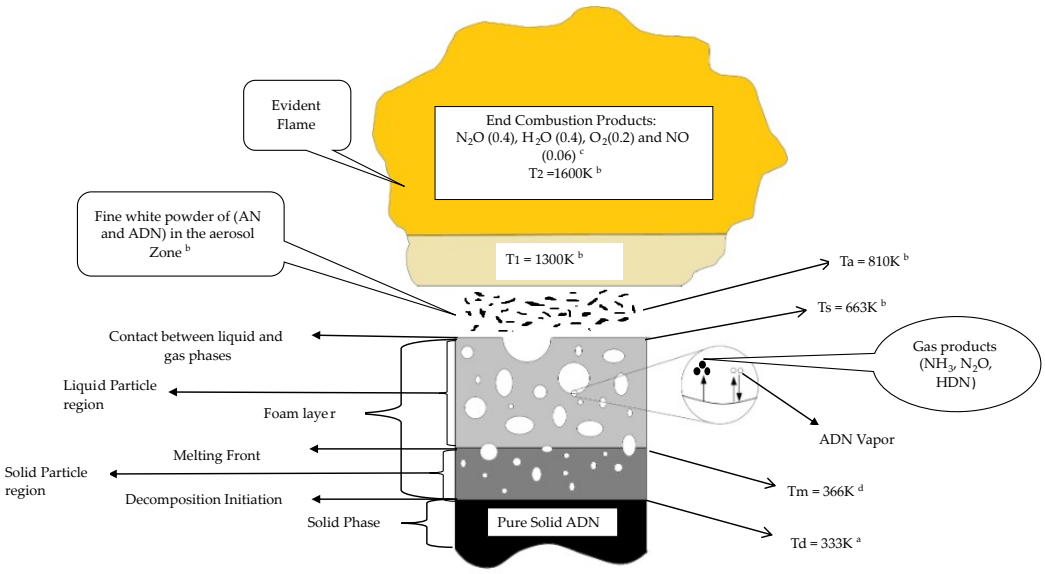

Figure 2. ADN monopropellant combustion wave structure schematic (not scaled; temperature representative of ADN flame at 5 atm), Data within figure was refered from [a] [28], [b] [73], [c] [75], [d] [79]; reproduced/adapted from [76] with permission from Elsevier.

5. Combustion of ADN with Metallic Fuels

Metals are an excellent choice as energy additives in space propulsion due to their high gravimetric and volumetric energy density and release of enthalpy. Their use in composite propellants increases the adiabatic flame temperature, resulting in enhancement of the specific impulse (I_{sp}). The metal oxides produced from metal combustion also inhibit combustion instabilities. However, metal combustion also poses certain challenges for their integration in composite propellants such as their resistance to ignition, uncertain combustion dynamics in both homogeneous and heterogeneous phases, very high increase in thermal fluxes, I_{sp} losses due to two-phase flows, slag accumulation, nozzle erosion, emission of plumes with metal oxides, etc. [82]. In the past decades, aluminium (Al) has been extensively used as a metallic fuel because of its high energy release in a variety of oxidation environments, high density, low oxygen demand, as well as due to its availability and low cost. Table 3 provides the physical and chemical properties of some metals, as well as a metalloid (boron), which have been explored as fuel additives in composite solid propellants. Among these, beryllium (Be) has the highest gravimetric heat release, but it has been banned due to its high toxicity and cost. Of the remaining metallic/metalloid fuels, boron (B) has the highest gravimetric and volumetric heat release, followed by aluminium (Al), magnesium (Mg), and titanium (Ti) in gravimetric heat release and titanium (Ti), aluminium (Al), chromium (Cr), and zirconium (Zr) in volumetric heat release. The oxygen consumption for boron (B) is the highest at 2.22, while it is 0.89 for aluminium and 0.66 for magnesium.

Table 3. Physical and chemical properties of various metal fuels; reproduced/adapted from [83] under license CC BY-NC-ND 4.0 by Elsevier B.V. on behalf of KeAi Communications Co., Ltd. (Beijing, China).

Element	Molecular Weight [g/mol]	Density [g/cm^3]	Ignition Temperature [°C]	Melting Point [°C]	Boiling Point [°C]	Combustion Heat per Mass O_2 [kJ/g]	Combustion Heat per Vol O_2 [kJ/cm^3]	Oxygen Consumption [a] [g_{O_2}/g_{Fuel}]
Al	26.98	2.70	>727	660.32	2519	31.063	83.870	0.89
Be	9.01	1.85	~2227	1287	2468	68.0	125.8	1.77
B [b]	10.81	2.34	1577–1727	2075	4000	58.968	137.985	2.22
Mg	24.31	1.74	627	650	1090	24.785	43.126	0.66
Cr	52.00	7.15	580	1907	2671	10.995	78.614	0.46
Fe	55.85	7.87	927	1538	2861	6.699	52.721	0.28
Ti	47.87	4.51	~1397	1668	3287	19.749	89.086	0.56
Zr	91.22	6.52	1467	1852	4377	12.03	78.436	0.35

[a] Defined as required oxygen in grams to oxidize 1 g of element; [b] Boron is metalloid.

5.1. Characteristics of Metal Combustion

Aluminium is one of the most common metallic fuels used in composite solid propellants, whereas magnesium is considered a low-power alternative to Al due to its easy ignition properties. The oxidation of the metalloid boron (B) generates high values of both volumetric and gravimetric heats of reaction, hence it can be considered for high-energy-density applications. Zirconium (Zr), with high density, can be considered to increase the density of the propellant and provide higher ΔV. Some studies also use metal hydrides (AlH_3, TiH_3) to increase the calorific content and specific impulse without increasing the combustion temperature. Combustion of metals in an oxygen environment is classified by the pathway of metal oxidation to its smallest suboxide [84]. When the metal fuel and oxidizer react in the gas phase, the combustion of metal fuel is governed by "vapour-phase reactions". The reaction of the outwardly diffusing gaseous fuel species with the gaseous oxidizer generates a high-temperature flame and the thermal diffusion to the condensed-phase fuel droplet surface sustains the fuel evaporation. However, when the metal reacts in the condensed phase, heterogeneous combustion occurs. The flame temperature in metal combustion is governed by properties of the reaction products such as metal oxides. For a few metals, their condensed-phase metal oxides form gaseous molecules of original metallic oxides, while many metal oxides volatilize by decomposition into gaseous suboxides and O_2 or O atoms. There is additional heat required to complete the vaporization and dissociation (or "volatilization") of metal oxides to convert them into the gaseous phase. The temperature associated with vaporization–dissociation of metal oxides is termed the "volatilization temperature", which can be referred to as the boiling point temperature of the metal oxide. The metals which have lower boiling point temperatures than their metal oxide's volatilization temperature follow the vapour-phase combustion pathway, otherwise heterogeneous reactions occur at the metal particles' surfaces. Table 4 highlights selected metals and their oxide's properties. Along with the boiling point temperature of the metal and their oxide's volatilization temperature, it also shows the standard heat of formation ($\Delta H_{f,298}$) and heat of vaporization–dissociation or heat of decomposition (ΔH_{vol}) of the metal oxides. The last column lists the total energy required to raise the temperature of the metal oxide to its boiling point temperature along with complete decomposition in the gas phase. If the heat generated from metal reactions at a given pressure and temperature is lower than the total energy required to volatilize the metal oxide, vapour-phase reactions occur, which limits the flame temperature up to the volatilization temperature of the metal oxides because the additional heat generated due to metal combustion is absorbed in vaporizing and decomposition of the metal oxides. This "limiting temperature" behaviour is associated with vapour-phase metal combustion only, not with heterogeneous metal combustion, because the boiling point temperatures of metals are higher than their oxides and the reaction products are already in gaseous form. In metal–oxygen systems,

the comparison between boiling points of metals and their oxides can help to determine the pathway of metal combustion. For example, the boiling point temperature of Al is well below the decomposition temperature of Al_2O_3; the oxidation of Al in an oxygen environment will occur in the vapour phase as a detached diffusion flame. However, the metalloid boron's boiling point temperature is higher than that of its oxide (B_2O_3), so the combustion occurs in a heterogeneous manner as there is enough energy available to vaporize B_2O_3, but it may not be enough to vaporize the metal. The magnesium–oxygen and titanium–oxygen systems behave similarly to the aluminium–oxygen system, while the zirconium–oxygen system behaves similarly to the boron–oxygen system. During the diffusion flame of the Al–oxygen system or similar vapour-phase combustion pathways, the flame temperature is limited to the volatilization temperature of the metal's oxides at equilibrium. In contrast the boron–oxygen or zirconium–oxygen system will not show behaviour that is limited by temperature .

Table 4. Various properties of selected metals and their oxides and nitrides; reproduced/adapted from [85,86] with permission from Elsevier.

Metal	Boiling Point T_{bp} [K] [a]	Oxide	T_{vol} [K] [b]	$\Delta H_{f,298}$ [kJ/mol]	ΔH_{vol} [kJ/mol]	$H_{T,vol} - H_{298} + \Delta H_{vol}$ [kJ/mol]
Metal Oxides						
Al	2791	Al_2O_3	4000	−1676	1860	2550
B [c]	4139	B_2O_3	2340	−1272	360	640
Mg	1366	MgO	3460	−601	670	920
Ti	3631	Ti_3O_5	4000	−2459	1890	2970
Zr	4703	ZrO_2	4280	−1097	920	1320
Metal Nitrides						
Al	2791	AlN	2710	−318	620	740
B [c]	4139	BN	4010	−251	840	950
Ti	3631	TiN	3540	−338	700	950

[a] T_{bp}: Metal boiling point at 1 atm. [b] T_{vol}: Volatilization temperature of oxides (stoichiometric combustion temperature creating compounds at P = 1 atm, T = 298 K). [c] Boron is metalloid

Table 4 also highlights the properties of metal–nitrogen systems, producing metal nitrides. Bucher et al. [87] experimentally investigated the combustion of a single, isolated aluminium particle in various pure quiescent atmospheres. The laser ignition of aluminium particles used electron-phase micro-analysis to estimate the condensed-phase products and their radial distribution. The formation of aluminium nitride was found in the fuel-rich region near the particle surface in nitrogen-containing atmospheres, such as (O_2/N_2) and N_2O. The equilibrium calculations suggested the presence of solid AlN at temperatures well above the melting temperature of aluminium oxides.

Micron-size aluminium (μAl; with the range of 10–40 μm) has been used for many decades in composite solid propellants to increase specific impulse as well as to eliminate combustion instabilities. Due to low volatility, metal particles can burn more slowly compared to other ingredients of composite propellants. Metal particles also show resistance to ignition due to formation of a protective oxide layer (oxide skin) on the surface. However, the ignition temperature of Al metal powder highly depends on the particle size, which was measured as 2300 K for micron-size Al to 900 K for nano-sized Al powder [88]. Additionally, the clustering effect of (μAl) under certain conditions can lead to the agglomeration phenomenon, forming larger particles and leading to incomplete combustion along with two-phase-flow effects. The clustering and agglomeration can form large droplets in the range of 50–200 μm, which require a long duration (approximately 10–100 ms) to burn completely. At certain conditions, Al combustion can become complex and can occur simultaneously in homogeneous and heterogeneous modes. For a typical propellant, metal powder is grouped together in the micro-structure of a solid propellant, with small metal particles filling space among large oxidizer particles in a binder matrix. The sequence of events in the combustion behaviour of Al particles in propellant flames

was explained in a simplified manner by Price [89]. With a rise in temperature, the metal particles emerge from the propellant burning surface in the presence of a melt layer of the binder and its decomposition products. These emerging particles experience concentration or accumulation. During the concentration process, the metal particles are continuously heated and sintered together by direct interaction. As the temperature increases beyond the melting point of the metal, particles and due to the protective oxide skin, the ignition is delayed. With continuous regression of the burning surface, these accumulations of metal particles are exposed to the evolving chemical and thermal environment. Further increases in temperature provide sufficient energy to break down the oxide skin, causing coalescence of these accumulations into agglomerates, either at the burning surface or near the burning surface, after detachment. The growing agglomerates have an outer layer in the more favourable hot zone and are ignited, and the agglomerates exhibit continuous coalescence along with inflammation towards the propellant surface. A glowing flame envelope is established on the growing agglomerate. When the inflammation reaches the propellant surface, the agglomerate completely detaches from the surface, producing smoke oxides and residual oxides. The spatial distribution of metal in the oxidizer/binder matrix and the properties of different ingredients of the propellant can lead to different hot sites and amounts of heat release, burn times, and distributions of metal oxides, which may ultimately impact the burn rate of the propellant and the combustion efficiency and combustion stability.

From the above discussion, it can be deduced that understanding the full potential of metal additives in composite solid propellants requires investigating various phenomena at a fundamental level, such as the metal ignition characteristics in the propellant matrix, the formation of condensed products and their agglomeration on the burning surface, the kinetics of metal combustion in the oxidizer, estimation of performance losses due to two-phase flow and slag formation, estimation of the exhaust signature, their lower cost and reduced sensitivities as well as explosion hazard, along with their longer self-life, estimating their environmental impact, and performing a life-cycle analysis. Traditionally, metal in ammonium perchlorate oxidizer has been used for more than six decades, leading to much fundamental understanding of metal (specially Al) combustion in the AP oxidizer. However, research into ADN-based composite solid propellants with metallic fuel has been conducted in recent decades. The use of Al metallic fuel in the traditional AP oxidizer can also lead to the formation of aluminium chloride ($AlCl_3$) along with HCl. ADN is considered a "green" chlorine-free solid oxidizer. ADN's burn rate is significantly higher than other solid oxidizers, but it shows instabilities and a scattered burn rate in the range of 2–10 MPa. The combustion behaviour of ADN in the presence other ingredients of composite solid propellants is of particular interest from the energetic point of view. In principle, the characteristic of the high burn rate of ADN can also lead to low aluminium agglomeration, due to increased proximity of possible high-temperature oxidizer–binder flames. Many recent studies related to ADN-based composite solid propellant have explored the impact of various additives on energetic performance, with a focus on replacing traditional toxic oxidizers and developing "green" composite solid propellants.

5.2. Performance of ADN-Based Solid Propellants with Metallic Fuel

Early experimental studies focused on the preparation of composite solid propellant based on ADN or double oxidizers, including non-energetic or energetic binders, and adding metallic fuel such as micron-sized Al (μAl). Mainly, the ballistic properties, thermal stability, and mechanical sensitivities (shock and friction) of these new propellants' were tested, along with a few small-scale motor tests. Chakravarty et al. [16] and Price et al. [90] investigated the burn rate of pure ADN laminae (in sandwich form) with

various compositions, including mono- and bi-modal fine and coarse ADN powders along with Poly-Butadiene Acrylonitrile acrylic acid (PBAN) binder and 10% Al powder, with sizes of either 30 μm Al or sub-micron (nano-sized) Al powder. The burn rates and pressure exponents of these compositions were compared with a similar AP composition in the pressure range of 0.68–10.34 MPa. At 2.07 MPa, the burn rate of AP/PBAN moderately increased with the addition of 10% sub-micron Al, while it moderately decreased with 30 μm sized Al powder. AP/Al did not ignite at 2.07 MPa. Pressed ADN showed a higher burn rate than pressed AP. Adding 10% Al powder of both sizes significantly increased the burn rates of pressed ADN, while adding Al to ADN/PBAN laminae did not affect the burn rate. The fine Al powder did not agglomerate and burn vigorously in the ADN/PBAN/Al composition, while coarse Al powder formed agglomerates. De Flon et al. [12] performed an initial evaluation on replacing AP with ADN for large space launch boosters. The theoretical calculations based on an ADN/HTPB/Al composite propellant showed an increase in specific impulse from 262 to 270 s, increase in characteristic velocity by 3.7%, and decrease in chamber temperature by 4%, when replacing AP with the same volume of ADN. Three formulations of 200 g composite solid propellant based on ADN/HTPB/Al were prepared and cured with isocyanate. The burn rate was measured for two compositions with 10 μm and one composition with 30 μm Al powder. The maximum burn rate of 12.8 mm/s was obtained at 6 MPa, with a pressure exponent of 0.9 for the ADN/HTPB/Al propellant prepared at a ratio of 64:20:16. Pang et al. [91] studied four compositions of propellants based on AP and ADN mixtures, while keeping the weights of other additives such as HTPB and Al the same. The ratios of AP and ADN were varied as 64:0, 54:10, 49:15, and 44:20. At pressures of 1, 4, 7, 10, and 15 MPa, experiments were conducted to determine the burn rates of the four samples. It was found that the burn rate increased with pressure increase as well as with an increasing percentage content of ADN. Around 15 MPa, the composition with AP/ADN as 44:20 had a burn rate and pressure exponent of 19.43 mm/s and 0.71, respectively. A decrease in density as well as flame temperature was also observed when increasing the percentage of ADN. The influence of the metal hydride AlH_3 on the ADN/GAP mixes' specific impulse was compared with Al additives by Gettwert et al. [92]. Their results stated that 85%, 87%, and 89% ADN solid loaded with 20% AlH_3 had specific impulses of 282, 285, and 288 s, respectively. Similarly, 20% Al with the identical materials and ADN loading produced an impulse of 273 s in all situations; however, 90% AP loading provided a specific impulse of 264 s. Rapid hydrogen release from metal hydrides can provide increased energy content and intensify the combustion. Additionally, the hydrogen release process can also leave the metal in a porous form, which increases its reactivity. Under the joint efforts of the HISP (High Performance Solid Propellants for In-Space Propulsion: 2011–2014) program in Europe, various studies were performed to increase the technological readiness level along with controlling the burn rate and pressure sensitivities of ADN/GAP/Al-based high-performing solid propellants. De Luca et al. [93] experimentally investigated the impact of various Al powders on composite solid propellant made of prilled ADN as the oxidizer, GAP as the binder, along with five variations of Al powders: micron-sized Al (μAl, two sizes: 5 μm and 18 μm) and nano-sized Al (nAl, 100 nm, with two coatings: naturally coated with Al_2O_3 and coated with stearic acid). All the ADN/GAP/Al samples had a composition ratio of 60:24:16. Additionally, the composite propellant ADN/GAP/AlH_3 was also tested with a composition ratio of 52:22:26. The burn rates were measured at various pressures within 0.1–10 MPa and compared with an AP/HTPB/metal composition of 68:14:18, with three types of Al powders: micron-sized Al (μAl, standard 30 μm), nano-sized Al (nAl, 100 nm with stearic coating), and activated-Al (act-Al, 3 μm), along with a 62.4:14:23.6 composition of AP/HTPB/AlH_3. The effects of various powder characteristics on AP suggest that the

burn rate of AP/HTPB/Al was increased by activated Al and it was further increased by nano-sized Al powder compared to micron-sized Al powder. However, with hydride (AlH_3), it increased significantly with a reduction in the pressure exponent. The burn rate range at 60 bar pressure was 7.1–13 mm/s for the studied AP/HTPB with Al powders with a pressure exponent range of 0.45–0.52, while it was 22.57 mm/s for AlH_3 with a pressure exponent of 0.33. The study compiled previous studies on ADN combustion, and highlighted ADN monopropellant's burn rate as 30 mm/s at 60 bar, with a pressure exponent of 0.6 [73], which was slightly reduced to the range of 0.46–0.6 within 2–40 MPa. It also highlighted the burn rate of an ADN/GAP (70:30) mixture at 60 bar as 22.23 mm/s, with a pressure exponent 0.49 [81]. The ADN/GAP/Al composition at 1 bar burns slowest with micron-sized Al (1 mm/s with 18 μm and 2 mm/s with 5 μm), followed by naturally coated nano-sized Al (3.1–3.8 mm/s), and AlH_3 (4.7–5.7 mm/s); while it burned fastest with stearic acid-coated nano-sized Al (9.5–18.5 mm/s), among the tested samples. These burn rate measurements at different pressures exhibited high-pressure exponents of 0.79 and 0.59 for micron-sized Al of 18 and 5 μm, respectively, leading to interpolated burn rates at 60 bar of 31.6 mm/s and 27 mm/s, respectively. The nano-sized stearic acid-coated Al powder was tested at 10 bar, with high burn rates between 23 and 62 mm/s and a pressure exponent of 0.44. AlH_3, at all pressure ranges, reduced the pressure sensitivity to the lowest (pressure exponent: 0.37), with a minor influence on the burn rate. The interpolated burn rate with the AlH_3 composition was 20.6 mm/s at 60 bar. Reviewing the above findings for ADN/GAP/Al and comparing the performances with AP/HTPB/Al, De Luca et al. [94] further suggested that dual-oxidizer systems (ADN+AP) or (ADN+AN), loaded with dual-metal fuels (μAl+nAl) or (μAl+AlH_3), along with a suitable binder can be a suitable choice to control both burn rates and pressure sensitivities for ADN-based solid composite propellants applicable for space propulsion application. Gogulya et al. [95] experimentally studied detonation characteristics to investigate the heat of explosion and mechanical sensitivities of ADN and ADN/Al mixtures. The 100 gms samples of prilled ADN (ADN_p) and crystalline ADN (ADN_c) were tested along with two kinds of Al powders: micron-sized commercially obtained spherical Al (Al_c, 15 μm) and ultra-fine nano-size Al (Al_n, 100 nm). The mechanical sensitivities were measured with critical pressure (P_{cr}) for detonation initiation. ADN_c (P_{cr} = 0.8 GPa) was found to have higher mechanical sensitivity compared to ADN_p (P_{cr} = 1.12 GPa). Addition of micron-sized Al (Al_c) to ADN_c (P_{cr} = 0.75 GPa) or ADN_p (P_{cr} = 0.85 GPa) led to a slight increase in mechanical sensitivity compared to pure ADN. The addition of nano-sized Al (Al_n) to ADN_c and ADN_p led to a significant increase in mechanical sensitivity, with P_{cr} = 0.23 GPa and 0.25 GPa. The measurement of detonation velocity for ADN_p had a maximum of 6.23 km/s at 1.6 g/cm^3 charge density and varied between 4.88 and 6.23 km/s for charge density variations of 1.2 to 1.785 g/cm^3. Due to increases and decreases in detonation velocity with charge density increases, the authors suggested that ADN belonged to the Group 2 Class High Explosives, as classified in [96]. The incorporation of commercial Al (Al_c) to prilled ADN (ADN_p) had no influence on the detonation velocity or pressure. For a short charge length (14.35 mm, density = 1.808 g/cm^3), the maximum detonation velocity observed was 5.65 km/s, while a longer charge length of 28.7 mm with the same density showed a reduced detonation velocity of 5.42 km/s, which further decreased below 3.5 km/s for a 56.62 mm charge length. It was found that the expanding deflagrating propellant (DP) of prilled ADN and Al_c had a surface temperature less than 3000 K in the first μs. Despite the reaction growth due to the addition of Al_c, there was no significant impact on the detonation propagation. The heat of explosion increased due to the addition of bigger-size Al_c particles, while the addition of nano-sized (Al_n) did not impact the heat of explosion.

Weiser et al. [97], motivated by a desire to understand the performance losses of metallized ADN-based composite solid propellant due to agglomeration and two-phase flow, theoretically and experimentally investigated the impact of replacing AP/HTPB with ADN/GAP in AP/HTPB/Al composite solid propellant. Table 5 describes the results of thermochemical calculations performed by using the ICT-Thermodynamic code [98] for AP/HTPB/Al and ADN/GAP/Al as well as another two combinations.

Table 5. Comparison of thermochemical equilibrium calculation results for AP/HTPB/Al and ADN/GAP/Al along other combinations; reproduced/adapted from [97] with permission from the author V. Weiser

Parameter	AP/HTPB/AI *	ADN/HTPB/AI *	AP/GAP/AI *	ADN/GAP/AI *
Density (kg/m^3)	1578	1522	1808	1753
P_c (Mpa)	7	7	7	7
T_c (K)	2357	2570	3624	3565
C_p $(J/kg-K)$	2047.2	2289.9	1918.2	2051.4
γ	1.29	1.28	1.26	1.26
Sound velocity (m/s)	1055	1106.1	1137.8	1190.5
C^*	1387	1458	1530	1593
$I_{sp}(s)$ in vacuum	271.3	279.6	291.1	300.3
$I_{sp}(s)$	247.4	257.5	265.5	274.7
Combustion products (chamber) (mol/kg)	47.45	51.07	36.64	40.32
Condensed products (chamber) (%)	8.64	14	7.77	7.29
Combustion products (nozzle) (mol/kg)	48.85	52.98	35.38	39.32
Condensed products (nozzle) (%)	17.6	18.75	8.38	7.54

* All compositions have oxidizer–binder–metal ratios of 60:24:16.

The theoretical comparison revealed that under standard conditions, gravimetric specific impulse was highest for ADN/GAP/Al compared to the other combinations. The density was slightly lower for ADN/GAP/Al than AP/GAP/Al. The condensed products were reduced significantly at the nozzle for ADN/GAP/Al (7.54%) compared to AP/HTPB/Al (17.6%). The combustion behaviour of ADN/GAP/Al was measured in the ICT window bomb at 0.1, 1, 3, 7, and 10 MPa, and agglomerate sizes were obtained by using a long-range microscope at 1 and 3 MPa. The data for the AP/HTPB/Al composition from [99] were used for comparison. The ADN/GAP/Al composite propellant was formulated by using 60% prilled ADN and 19.59% GAP-Diol along with the isocyanate curing agent 3.1% Desmodur E305, 1.31% alkaline curing agent bis-propargyl-succinate (BPS), and 0.04% curing catalyst dibutyltin dilaurate (DBTDL), along with four different kinds of aluminium powders, as shown in Table 6.

Table 6. Composition of ADN/GAP/Al composite solid propellant and types of Al powder used; reproduced/adapted from [100], with permission from Springer.

ADN [a]	GAP-Diol	E305 [b]	BPS	AI	DBTDL [c]	NCO/OH [c]	BPS/OH [c]
60%	19.59%	3.1%	1.31%	16%	0.04%	0.56%	0.8%
Aluminium Type and Size							
A-81		Alcan 400		nAl,Al_2O_3		L-Alex [d]	
18 μm		5 μm		100 nm		100 nm	

[a] Prills 208 μm, ICT-Fraunhofer; [b] Desmodur; [c] Catalysts are not included in the final formulation; [d] Stearic acid-coated before exposure to air.

All compositions were ignited at atmospheric pressure (0.1 MPa) and burned with a linear regression rate. The burn rate at 0.1 MPa increased 2 times from sample to sample, with 18 μm Al having the slowest burn rate, followed by 5 μm Al, uncoated 100 nm Al, and

stearic-coated 100 nm Al had the highest burn rate. When comparing with AP/HTPB/Al composite propellant, ADN/GAP/Al had burn rates 3 to 4 times higher over the standard pressure range. At higher pressure, samples with nano-aluminium burnt inside–out with expulsing flames, exhibiting porous combustion behaviour. The burn rates were measured for only micron-sized Al (5 μm and 18 μm) propellants at high pressures (1–10 MPa); it varied linearly (on a log–log scale) with increases in pressure. The average agglomerate size for ADN/GAP/Al propellant with micron-sized Al was found to be independent of the initial Al powder size at measured pressures of 1 and 3 MPa. However, the average agglomerate size was larger for ADN/GAP/Al propellant (approximately 165–167 μm at 1 MPa and 126–129 μm at 3 MPa) than for AP/HTPB/Al. This behaviour is attributed to GAP's presence creating a porous burning surface, trapping the particles, allowing larger size agglomeration, based on similar observation on AN/HTPB/Al formulation in previous studies. The specific impulse losses due to two-phase flow are computed by using the following equation:

$$(\Delta I_{sp})_{2P} = C_3 \frac{\xi_{cc}^{C_4} d_P^{C_5}}{P_{cc}^{0.15} \varepsilon^{0.008} d_t^{C_6}}$$

where ξ_{cc} is the computed molar fraction of condensed-phase products in the combustion chamber (mol/100 g), d_P is the averaged diameter of condensed particles (μm), P_{cc} is the combustion chamber pressure (psi), ε is the geometric expansion ratio of the nozzle, d_t is the throat diameter (inch), and C_3, C_4, C_5, and C_6 are correlation coefficients depending on the type of propulsive unit and particle mean diameter. To compare with AP/HTPB/Al, the correlation coefficients used were the same as for the AP/HTPB/Al agglomerates ($C_3 = 7.58$, $C_4 = 0.5$, $C_5 = 0.8$, $C_6 = 0.33$) [99]. The calculation shows that the impulse losses are higher due to larger agglomerate sizes, varying from 50 to 67 s at 1 MPa and with a standard nozzle.

Weiser et al. [100] further continued their previous study for ADN/GAP/Al composites (only with 18 μm Al powder), as listed in Table 6, including a bi-modal ADN mixture of ratio 70:30 with coarse (208 μm) and fine (55 μm) ADN prills. The burn rates were measured in a nitrogen environment in an ICT window bomb with additional measurements. The propellant burning rate was measured with a higher number of sample points between a pressure range of 0.1 and 15 MPa. The Al agglomeration behaviour was investigated at pressures of 0.1, 1, 3, and 5 MPa, with Al sample collection at different locations from burning strands for FE-SEM and elemental analyses. The temperature was also estimated using near-infrared radiation (NIR) spectra. The burn rate at 7 MPa was observed as 29.6 mm/s, a linear increase in the burn rate was observed with pressure on a log–log scale, showing a pressure exponent of 0.58. The maximum temperature measured at 0.1 MPa was 2000 K, which increased up to 3000 K at pressures above 10 MPa. When compared with the adiabatic temperature from ICT-code calculations, the measured temperatures were 20–30% lower than the calculated ones due to non-adiabatic conditions and heat losses. Figure 3 shows the axial temperature profiles at different pressure levels, obtained from emission spectra, and Figure 4 shows the maximum temperature dependence on pressure. Two flame zones are considered: (1) a zone close to the surface, where agglomeration takes place; and (2) a zone including moving hot particles, where detached aluminium-rich particles are oxidized by gases in the flame zone. Up to pressures of 5 MPa, the temperatures near the surface are lower than in the flame zone. The flame zone temperature rises from 2200 K to 2650 K at 5 MPa, while the temperature of the near-surface zone rises from 1850 K at 0.1 MPa to 3000 K at 15 MPa. At high pressures, above 5 MPa, the flame shifts towards the burning surface along with the oxidation zone of particles, producing higher temperatures near the burning surface. In the observed cases, most of the particles glow up to a maximum of 15 mm from the burning surface.

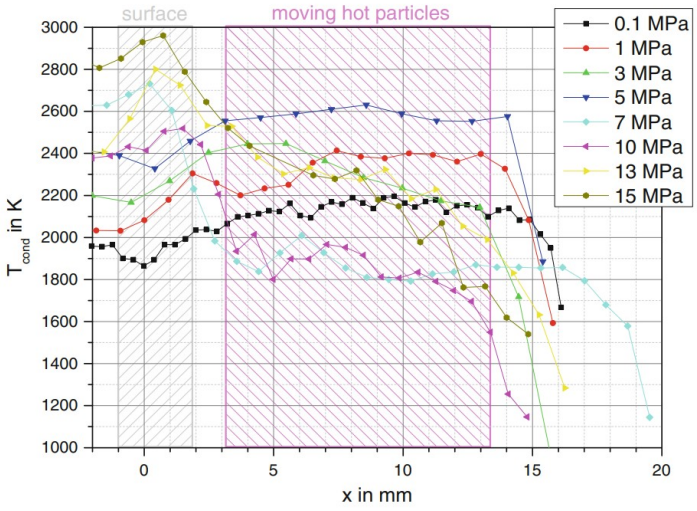

Figure 3. The axial plots of continuum temperatures at different pressure levels for ADN/GAP/Al combustion; reproduced/adapted from [100] with permission from Springer.

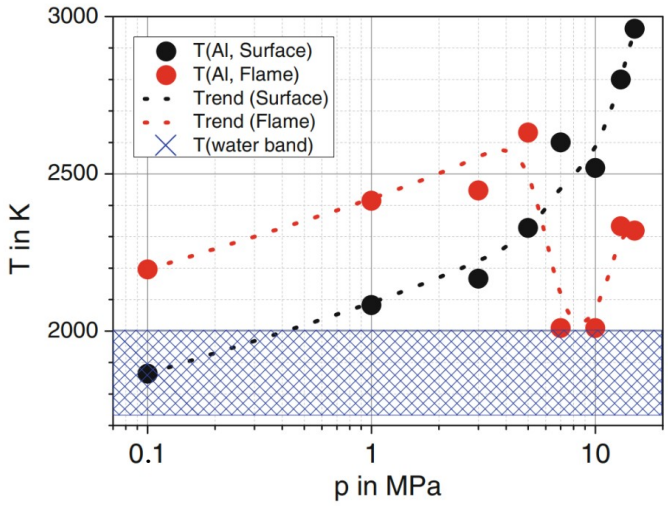

Figure 4. The maximum temperature obtained near the surface and in the flame zone as a function of pressure; reproduced/adapted from [100], with permission from Springer.

The agglomeration phenomenon was observed and quantified by video analysis. In the pre-aggregation stage, the average diameter of particles grew up to 77–78 μm, which was almost 4–5 times the size of the original Al powder (18 μm). Interaction with neighbour particles and rolling on the burning surface led to increases in the agglomeration sizes. The particles detached from the burning surface after reaching a certain size and showed turning movement in a straight line after lift-off. The mean diameter of detached agglomerates reached 265 μm at 0.1 MPa, while it was less than 150 μm at 5 MPa for bi-modal ADN samples. The particle size of the ADN oxidizer impacts the observed agglomerate size rather than the Al powder particle size. Comparing mono-modal samples with ADN prills of mean diameters between 208 μm and 228 μm, an increase of 10% in the mean diameter of ADN leads to a 2 times increase in agglomerate size at 1 MPa, using the same size of Al powders. The samples tested with 5 μm and 18 μm Al powders, did not show significant differences in agglomerate sizes at all pressures up to 3 MPa. SEM analysis of the collected sample suggested incomplete combustion at 0.1 MPa due to the presence of an oxide cap. With increased pressure, more complete oxidation occurred. Most particles collected at all pressure levels showed pore formations due to gas release from particles.

Further, Gettwert et al. [101] performed lab-scale rocket motor tests with 64 mm grain diameter for non-metallized ADN/HMX/GAP (58.5%:11.5%:25.5%, plasticizer: 4.5%) and ADN/FOX12/GAP (50%:20%:25.6%, plasticizer: 4.4%) along with metallized ADN/GAP/Al (60:24:16), and compared with standard AP/HTPB/Al (68%:9.55%:18%, plasticizer: 4.1% and additives: 0.4%) compositions. FOX12 is guanylurea dinitramide (GUDN), which is considered an insensitive high explosive. The experimentally measured gravimetric specific impulses are shown in Figure 5a, along with computed volumetric specific impulses in Figure 5b.

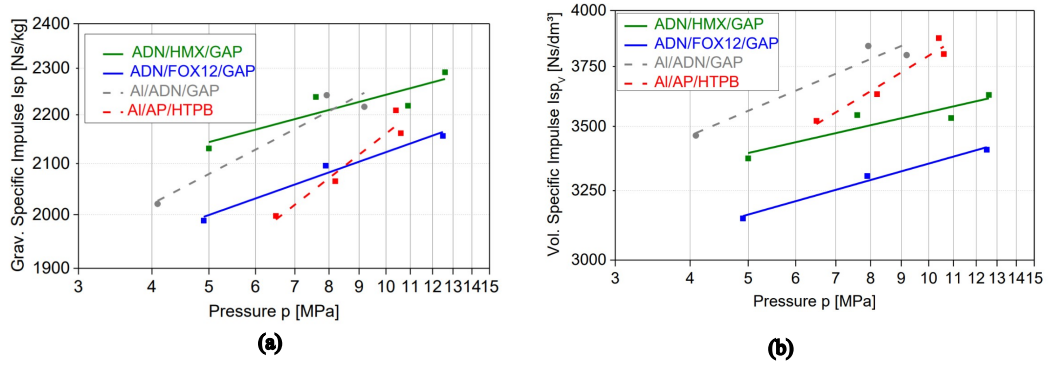

Figure 5. (**a**) Gravimetric specific impulse obtained from experiments at different pressures. (**b**) Volumetric specific impulse at different pressures calculated from experimental gravimetric I_{sp} and the densities of the propellants. Reproduced/adapted from [101], with permission from the author V. Gettwert.

According to the findings, AP/HTPB/Al produced a lot of smoke; however, aluminized ADN/GAP had no secondary signature, while non-aluminized ADN/GAP propellants showed no visible signature. ADN/GAP/Al and ADN/HMX/GAP outperformed AP/HTPB/Al for gravimetric specific impulse at all pressure levels, and ADN/FOX12/GAP performed better in the lower pressure range. The volumetric specific impulses for aluminized propellants are higher than for non-aluminized ones, while ADN/GAP/Al had better performance than AP/HTPB/Al up to 10 MPa. Based on thermodynamic calculations, it was found that the non-aluminized propellants were usually less dense and had lesser chamber temperatures. ADN-based propellants had higher burn rates in comparison with AP/HTPB/Al, as shown in Figure 6, which shows the burn rate variation with pressure for different propellant formulations using lab-scale rocket motor tests (in Figure 6a) as well as in a Crawford bomb (in Figure 6b). The minor differences in pressure exponents between the two tests suggests the importance of performing both tests for new propellants. The study also conducted standard shock sensitivity (gap test), friction and impact sensitivity, and chemical and thermal stability tests for ADN/GAP-based propellants. It was concluded that ADN/GAP-based propellants have potential for use as high-energy, low-signature propellants. The combination of ADN with the less sensitive FOX12 can provide an alternative to double-base low-signature propellant for tactical rockets.

Under the GRAIL (Green Advanced High Energy Propellant for Launchers) project, with the ambition to develop a safe, low-cost, and high-performance green solid propellant, 24 formulations of AN/ADN-based double-oxidizer propellants were explored by Gettwert et al. [102] in initial reporting. A bi-modal mixture of coarse and fine spherical ADN prills (with sizes of 48 µm, 212 µm, and 218 µm) was used as oxidizer. The phase-stabilized AN was used in spherical form. The Al amount was fixed to 18% in every formulation. Finer Al powder (size 4 µm) and medium Al powder (20 µm) were used for better processing. Four binders, HTPB, GAP, Desmophen2200 (polyester), and GAP/Desmophen2200 (80:20)

were included, along with an energetic plasticizer and selected curing agents. Initial thermodynamic calculations using the ICT-code were performed to calculate the specific impulse at a chamber pressure 7 MPa and nozzle expansion of 70:1. Also, the amount of oxidizer needed to obtain the maximum I_{sp} performance for a given composition was determined by calculations. The ADN/AN ratio in the dual oxidizer was varied from 100/0 to 0/100, while keeping other constituents the same. It was found that 100% ADN gave the best performance (highest calculated I_{sp}) with all additives. The 100% AN had a higher calculated specific impulse performance with the GAP and GAP/Desmophen2200 binders compared to AP/HTPB/Al, while it was lower with the HTPB and Desmophen2200 binders. Finally, solid loadings (oxidizer and fuel) of 78%, 75%, 83%, and 78% were achieved to prepare the final testing formulations with GAP, GAP/Desmophen2200, HTPB, and Desmophen2200, respectively. In each formulation, the ADN/AN ratio varied from 100/0, 90/10, 70/30, 50/50, 30/70, and 0/100 to measure burn rates at pressures 1, 2, 4, 7, 10, and 13 MPa. These burn rates were used to calculate the pressure exponents and burn-rate relations. From the initial measurements, it was found that increasing the AN constituent in ADN/AN dual oxidizers leads to a decrease in burn rates, without impacting the theoretical value of I_{sp} significantly. The measured burn rates at 7 MPa conditions reduced from 43.9 to 4.3 mm/s, 22.0 to 4.0 mm/s, 13.8 to 2.8 mm/s, and 14.7 to 2.9 mm/s for GAP, GAP/Desmophen2200, HTPB, and Desmophen2200 binders with an increase in AN content. The pressure exponent varied significantly for the HTPB and Desmophen2200 binders, between 0.3 and 1.52 and 0.75 and 1.07, respectively, initially increasing with increases in AN content, then decreasing when more than 30% AN is mixed in. For GAP and GAP/Desmophen2200, the pressure exponent remained in the ranges of 0.62–0.8 and 0.61–0.76, respectively. These studies were further extended in [103,104], following a similar methodology of theoretical ICT-code calculations to determine the solid loading for the maximum I_{sp} and producing the propellant formulation by varying the ADN/AN ratio while keeping the metal content the same. The burn rate measurements were performed with pressure exponent computation to achieve a target burn rate between 7 and 15 mm/s at 7 MPa and a pressure exponent lower than 0.6 for space application. Additionally, Tagliabue et al. [103] performed friction and impact sensitivity along with compatibility tests between ADN and the phase-stabilizing AN agent, as well as a thermal stability test by varying the AN content in the mixture with GAP and HTPB binders along with bis-azido-triethylene-glycol (BATEG) and di-octyl-adipate (DOA) plasticizers, respectively. The findings suggested that the burn rate decreased with increases in AN content for all compositions. The pressure exponent for the ADN/AN/GAP/Al/BATEG propellant still remained between 0.62 and 0.73 and the ADN/AN/HTPB/Al/DOA propellant between 0.31 and 1.52, while showing a pressure exponent lower than 0.6 for compositions with high AN contents and burn rates below 3 mm/s. Phase stabilization with KNO_3 was found to be compatible with prilled and coated ADN prills, while the phase stabilizer NiO caused decomposition of ADN. The study suggested using a burn-rate modifier with ADN/AN/GAP/Al propellant to achieve the target burn rate and pressure exponent based on ADN/AN ratios of 70:30 or 60:40. The next study by Gettwert et al. [104], focused on the composition ADN/AN/GAP/Al with bi-modal ADN and phase-stabilized AN (for both oxidizers, coarse–fine = 70:30), a GAP-diol binder cured by isocyanate, along with the reaction catalyst dibutylyltin dilaurate (DBTDL) and various inert plasticizers: dibutyl sebacate, plasticizer (unknown, due to military use). The measured burn rate for ADN/AN/GAP/Al/dibutyl sebacate propellant with an ADN/AN ratio of 50:50 was 10.5 mm/s at 7 MPa, but the pressure exponent was too high at 0.83. A similar propellant with ADN only had a higher burn rate of 16.8 mm/s at 7 MPa, with a desirable pressure exponent of 0.57. The composition ADN/AN/GAP/Al/unknown plasticizer,

with ADN/AN = 100:0, exhibited a burn rate of 15.2 mm/s at 7 MPa, while it had a pressure exponent of 0.46 within the 4–13 MPa pressure range. A similar composition with ADN/AN = 70:30 exhibited a burn rate of 14.01 mm/s and a pressure exponent 0.62. Based on the last composition, the AN oxidizer was further modified by removing fine powder of AN from the bi-modal composition and the ratio of coarse to fine ADN was changed to 30:70 to compensate for the removal of fine AN particles. This composition with changed ADN and AN powder size burned at 13.71 mm/s at 7 MPa, with a pressure exponent 0.64. These studies on ADN/AN dual oxidizers paved the way for integrating ADN-based "green" solid propellant for space applications by replacing AP/HTPB/Al propellant without much deviation from the desired targets.

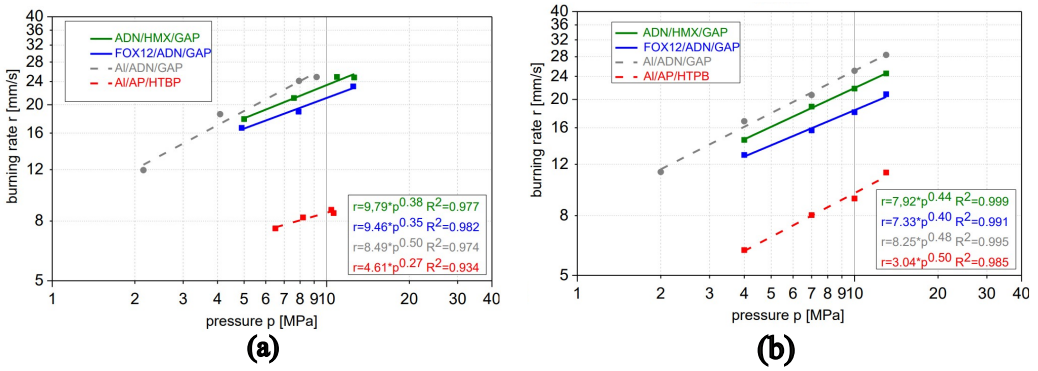

Figure 6. Burn rates from the (**a**) lab-scale rocket motor and (**b**) Crawford bomb tests at different pressures; reproduced/adapted from [101], with permission from the author V. Gettwert.

Pozzoni et al. [105] conducted technical feasibility tests with thermochemical simulations to replace AP/HTPB/Al-based solid propellant in the EAP boosters of the Ariane 5 launcher. Three novel ADN-based compositions were investigated. The thermophysical properties, motor performance, and combustion product analysis were conducted by using the NASA CEA code according to the nozzle exit area and desired thrust profile of the EAP booster mission for 60 km altitude within 130 s. The burn characteristics and compositions for the three propellants along with an AP-based propellant for the EAP booster are shown in Table 7.

Table 7. Burn characteristics and composition of studied propellants and calculated performance parameters for the mission objectives of EAP booster (last three columns); data from [105].

Propellant	Composition	Density [g/cm³]	a [mm/(sbar^n)]	n [−]	r_b@60 bar [mm/s]	Max. Burn Rate [mm/s]	Mean Burn Rate [mm/s]	Mean I_{sp} [s]
EAP	68% AP + 14% HTPB + 18% Al (Formulation of Ariane 5 EAP boosters)	1.71 [93]	1.08 [93]	0.46 [93]	7.1 [93]	7.1	6.0	264.4
ADN59	55% ADN + 30% HMX + 19% GAP + 13.4% TMETN [a] + 1.6% stabilizers (Double oxidizer ADN/HMX)	1.63 [93]	2.37 [93]	0.52 [93]	20 [93]	15.5	12.9	250.1
ADNAN55	30% ADN + 30% AN + 16.13% GAP + 3.3%BATEG + 18% Al + curing agents (Double oxidizer ADN/AN)	1.84 [103]	0.61 [103]	0.71 [103]	11.2 [103]	11.4	9	270.4
ADNAN55 BI-BI	30% ADN + 30% AN + 12.9% GAP + 3.25% D2200 + 3.3% BATEG + 18% Al + curing agents (Double oxidizer ADN/AN and double binder GAP/D2200)	1.83 [106]	0.42 [106]	0.77 [106]	9.8 [106]	10.0	7.6	268.4

[a] TMETN: Trimethylolethane trinitrate.

The vacuum and optimal thrust calculations for all formulations at various altitudes (of EAP booster mission profile), chamber pressures, and nozzle expansion ratios while keeping the exit area the same revealed that ADN59 propellant results in the highest thrust (maximum in range of 14–16 MN), while the thrust produced by ADNAN55 and ADNAN55 BI-BI

is (maximum in range of 8–9 MN) comparable to the AP-based propellant for the EAP booster. The higher thrust generated by ADN59 is due to the lower nozzle expansion required for ADN59 compared to other propellants, which leads to a higher throat area for a fixed exit area of the nozzle and overall higher mass flow rate. Table 7 also shows the computed maximum and mean burn rates for all four propellants during the desired mission profile. Although the pressure exponent n of ADNAN55 and its BI-BI formulations are lower than 1, they are still higher than the pressure exponent of the EAP booster, while ADN59 is closer to the EAP formulation. ADN59 presents a higher burn rate than required (7–15 mm/s), while the ADNAN55 BI-BI formulation was found to be the best among the three, which have maximum and mean burn rates closer to the EAP booster. The maximum and mean chamber pressure and temperature are found to be lower for ADN59 propellant (mean pressure was 16 bar lower and temperature was 300 K lower), while ADNAN55 BI-BI propellant has maximum and mean pressures and temperatures slightly higher than the EAP booster (mean pressure was within 1 bar and temperature was within 60 K). Table 7 also shows the mean specific impulse obtained for all compositions, with ADN59 having the lowest I_{sp}, requiring 4.9% more propellant mass compared to the mass of the propellant for the EAP booster (227 tons), while ADNAN55 and ADNAN55 BI-BI show 2.2% and 1.5% reductions in the required propellant mass, respectively. All three ADN-based compositions show excellent performance, with characteristic velocities c^* of around 1600 m/s, which is slightly better than the c^* of the AP-based propellant (about 1578 m/s).The study also evaluated the combustion product compositions with a shifting equilibrium approach through the divergent section of the nozzle. Figure 7 shows the compositions of the combustion products for all four propellants. HCl is not present in ADN-based propellants and aluminium oxide α-Al_2O_3 is not present in ADN59, a non-aluminized composition. Because of having the same Al loading, all aluminized propellants show no difference in α-Al_2O_3. CO production was significantly high in the EAP booster; this was reduced to almost half in all the ADN-based propellants. ADN59 produced very high CO_2, whereas it was only 2% in the EAP booster and 3% in ADNAN55 and its BI-BI formulation. Overall, it was concluded that using aluminized ADN-based propellants (ADAN55 or ADAN55 BI-BI) can reduce toxic HCl emissions by 47.8 tons, CO by 26 tons, and increase CO_2 emissions by 2.7 tons while replacing the AP with ADN based formulation in EAP booster, and the remaining reaction products are only water, N_2, and H_2.

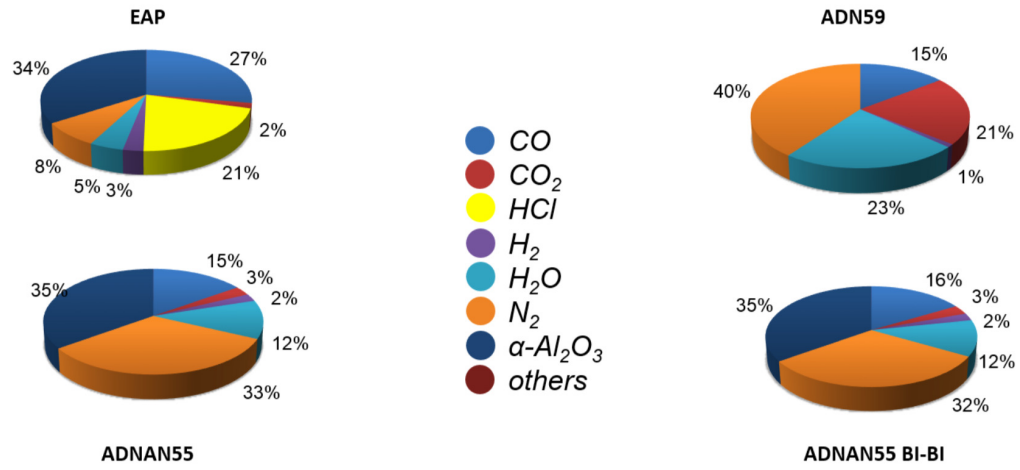

Figure 7. Combustion product composition calculated for AP- and ADN-based propellants; reproduced/adapted from [105].

5.3. Effect of Morphology and Micro-Structure on ADN–Metal Combustion

The above studies mainly focused on adding micron-sized aluminium powder to ADN-based composite propellant and finding compatible binders and additives, with the aim of optimizing burn rates as well as pressure exponents. A few studies have also explored the application of nano-sized aluminium powder and aluminium hydride to enhance the burn rate of composite solid propellant. It is understood that morphology and micro-structure, along with various mutual interactions and compatibilities among propellant ingredients, can have a significant impact on the combustion behaviour of composite solid propellant. These properties depend upon the adopted fabrication process as well as having an impact on the mechanical and thermal stability of the propellants. Various surface modification techniques such as micro-encapsulation, ultrasound sonication, fluidized-bed coating, and solution-coating methods have been adapted for ADN, with the target of increasing its anti-hygroscopic properties in combination with different coating materials. Another approach, co-crystallization, has also been explored to modify the hygroscopic characteristics, thermal stability, and mechanical sensitivities of ADN mixes. Details of these approaches are given in [10,21,107]. In this section, studies exploring the effects of morphological and micro-structural changes of composite propellants on their thermal oxidation are mainly reviewed. To avoid the toxic and incompatible (with ADN) isocyanate curing agent, Gong et al. [108] used a propargyl-terminated ethylene oxide-tetrahydrofuran copolyether (PTPET-A3) binder with two types of ADN particles and RDX and Al to prepare composite solid propellants. Spherical ADN (ADN_s, diameter 5–20 μm) and flaky ADN (ADN_f, size 10–50 μm and thickness: 1–3 μm) were used. The morphology of the prepared composites was observed using SEM, which suggested the uniform distribution of ADN_s, while ADN_f was not well distributed due to the observed high viscosity and poor processing properties during fabrication of ADN_f. The mechanical properties of ADN_s were found to be significantly better than ADN_f. The burn-rate measurements were performed between pressures of 3 and 17 MPa. The burn rate for ADN_f/PTPET-A3/RDX/Al (30%/28.5%/14.5%/5%) was found to be higher (7.8–29.8 mm/s) at each pressure level than for ADN_s/PTPET-A3/RDX/Al (30%/28.5%/14.5%/5%), being 6.95–19.70 mm/s. The pressure exponent for flaky ADN was 0.783, while spherical ADN showed two branches and different pressure exponents at lower and higher pressure ranges: 0.364 (3–11 MPa) and 1.256 (11–17 MPa). For ADN_f, the flame structure showed bright larger Al particles adhering to the surface, while the ADN_s flame structure showed small Al particles in large quantities in the flame zone. Xin et al. [109] employed a high-pressure differential scanner (HP-DSC) to examine the influence of nano-Al versus nano-Al coated with glycidyl azide polymer (GAP) on the thermal decomposition of ADN. A silane coupling agent (KH-550) was utilized as an interface between the GAP and the nano-Al to create a core–shell nano-Al/GAP, along with ultrasound blending to produce nano-Al/ADN and nano-Al/GAP/ADN combinations. The findings demonstrated that both nano-Al as well as coated nano-Al/GAP enhanced the temperature-associated decomposition of ADN. Further, Xin et al. [110] employed mechanical ball-milling, creating nano-Al by minimizing the chloride form of aluminium anhydrous via lithium aluminium hydride. The thermal decomposition of ADN and the n-Al/ADN composite was explored by HP-DSC, and it was discovered that nano-Al had very little impact on ADN's melting temperature, while the decomposition temperature of n-Al/ADN increased significantly and exhibited a single peak in the DSC plot. The effect of micron-sized and nano-sized Al powder particles on ADN's thermal safety characteristics were studied by Lei et al. [111] by experimental measurements including DSC, accelerating rate calorimetry (ARC), and slow cook-off, as well as deflagration point tests. It was suggested that the presence of Al accelerates the process of decomposition to combustion of ADN, which leads to reduced thermal safety of ADN. The $n-$Al has a greater impact on the

thermal safety characteristics of ADN than μAl. In order to understand the mutual influence of Al and ADN on each other, core–shell structured micro-composites were prepared by an in situ crystalline growth method, with Al particles (average particle size: 5 μm) as the core and ADN as the shell (Al@ADN) by Li et al. [112]. SEM, X-ray diffraction (XRD), and thermo-gravimetry analysis (TGA), as well as differential scanning calorimetry (DSC), were employed to investigate the shapes, structures, and thermal behaviour of Al@ADN. The chemical compositions and structure were investigated employing X-ray spectroscopy (XRS) and SEM after heating up. A high-speed camera recorder was used to capture the combustion characteristics of Al@ADN in an O_2 environment. Two different mass ratio powders of Al:ADN, 5:1 and 10:1, were investigated. Figure 8 summarizes the overall process followed in the study. The SEM and XRD images before heating show that pure Al particles have a spherical shape with a very thin oxide layer, observed due to traces of O. ADN was found to be evenly distributed on the Al surface for both the compositions. The DSC, TGA, surface composition, and morphology of samples provides the mechanism of thermal oxidation of Al@ADN. When the temperature of Al@ADN increased near to 90 °C, ADN dots on the surface started melting to form liquid, leading to a decrease in density. An increase in temperature to 250 °C caused ADN to go through many decomposition reactions, forming HNO_3 or $HN(NO_2)_2$, which first corroded the alumina layer, while nitric acid diffused inside and reacted with exposed Al, forming aluminium nitrate ($Al(NO_3)_3$), which decomposed to form alumina and amorphous alumina and grew. Below the melting point of Al (∼660 °C), the amorphous Al transformed to γ-Al_2O_3, and oxygen from the outside slowly started oxidizing the exposed Al. Beyond 660 °C, inner Al melts moved outwards and broke the surface alumina shell, and γ-Al_2O_3 was transformed to α-Al_2O_3. Higher temperatures led to further growth of α-Al_2O_3. The following reactions occurred during the interaction of Al and ADN apart from ADN decomposition:

$$Al_2O_3 + 6\,HNO_3 \rightleftharpoons Al(NO_3)_3 + 3\,H_2O$$
$$Al + 4\,HNO_3 \longrightarrow Al(NO_3)_3 + NO + 2\,H_2O$$
$$4\,Al(NO_3)_3 \rightleftharpoons 2\,Al_2O_3 + 12\,NO_2 + 3\,O_2$$

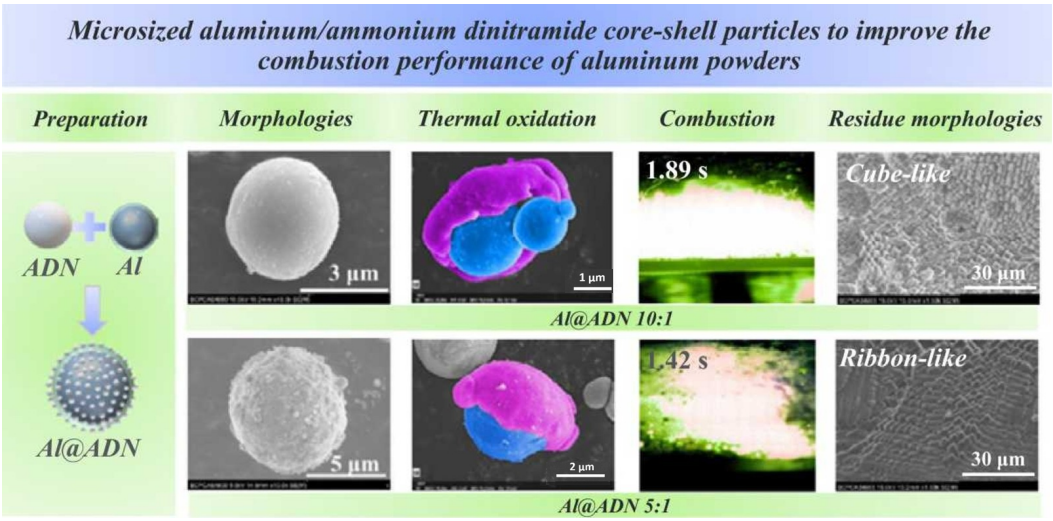

Figure 8. Summary of thermal oxidation and combustion of Al@ADN; reproduced/adapted from [112] with permission from Elsevier.

To study their combustion behaviour, 100 g samples of Al and Al@ADN were ignited in a transparent quartz tube at atmospheric oxygen with a flow rate of 10 L/min. Table 8 shows the ignition and burn time of each sample. The ignition time is the time between switching

on of the ignition and the start of firing of the sample, while the burn time is the time between the onset of firing and the natural extinguishing time. Pure Al cannot be ignited in these experimental settings. Both Al@ADN 10:1 and Al@ADN 5:1 were ignited easily in the presence of O_2 with a bright glaring flame, as shown in Figure 8. Al@ADN 5:1, with a higher content of ADN, was ignited quickly and burned quicker than Al@ADN 10:1. SEM images of the combustion product shows a cube-like structure (size: ∼3 µm) for Al@ADN 10:1, while Al@ADN 5:1 has a ribbon-like structure (size: ∼3 µm, length: ∼10–50 µm). Both residues are composed of Al and O according to elemental maps. EDS analysis shows that Al@ADN 5:1 has a higher oxidation degree. The XRD pattern shows production of α- and γ-Al_2O_3, without the presence of Al. The ratio of α- to γ-Al_2O_3 is higher for Al@ADN 5:1 compared to Al@ADN 10:1.

Table 8. Ignition and burn times for Al@ADN 10:1 and Al@ADN 5:1; reproduced/adapted from [112], with permission from Elsevier

Sample	Ignition Time (s)	Burning Time (s)
Al	no ignition	-
Al@ADN 10:1	1.83	8.41
Al@ADN 5:1	1.09	6.16

Recently, Zhang et al. [113] explored a surface modification method by producing energy-containing ADN microspheres. The suspension assembly process was used to coat ADN with GAP (G-ADN), fluorine rubber F2602 (F-ADN), or hydroxyl-terminated block copolyether HTPE (H-ADN). The crystal and chemical morphology (SEM, FTIR) of the microspheres, and mechanical sensitivity and hygroscopic tests as well as thermal decomposition and combustion analysis were performed for pure ADN and G-ADN, F-ADN, and H-ADN. The SEM analysis showed that the suspension assembly process led to a high degree of sphericity, with particle sizes concentrated in a narrow band of 20–30 µm. The FTIR results suggested that the chemical structure of ADN was not altered in all cases. F-ADN and H-ADN showed higher thermal stabilities in DSC measurements than pure ADN; G-ADN had lower thermal stability. The critical impact sensitivity for pure ADN was 7J, while it increased to 13, 17, and 15 for G-ADN, F-ADN, and H-ADN, respectively. The friction sensitivities also improved significantly, in a similar order. A moisture absorption test was conducted to evaluate the hygroscopicity of the prepared samples. At 25 °C and 60% relative humidity, the moisture absorption value of raw ADN was as high as 66.67%, while it reduced to 40%, 9.43%, and 12.12% for G-ADN, F-ADN, and H-ADN, respectively. F-ADN's low hygroscopic nature is due to formation of a dense encapsulation layer on ADN's surface. The raw ADN and coated ADN (61%) were pressed into Φ 6 mm × 3 mm pellets with compositions of Al (18%) powder and binder of poly-tetrahydrofuran (PBT) (8.4%), plasticizer of bis(2,2-dinitropropyl) acetal (A3) (11.7%), and curing agent of toluene diisocyanate (0.4%). The combustion characteristics were evaluated only with qualitative visualization and average burn times were measured as 1.353 s, 1.513 s, 1.578 s, and 1.673 s for pure ADN, G-ADN, F-ADN, and H-ADN, respectively. F-ADN was also tested after hygroscopic treatment, showing a longer burn time of 5.033 s and a bright flame with a distinct flame edge. Overall, the study suggested that the use of fluorine rubber-encapsulated ADN provides a viable option for ADN-based composite solid propellant. Similarly, Qiao et al. [114,115] utilized co-crystallization techniques to produce ADN co-crystals with anti-hygroscopic properties and performed thermal and mechanical sensitivity analyses along with hygroscopic testing to obtain the desired properties, but the combustion behaviour with pure or with composite metal fuels was not tested. The energetic performance was evaluated by performing thermochemical calculations. The ADN-18C6 [114] (18-crown-6) co-crystalline supramolecule was prepared using the solvent

evaporation method with a 1:1 ratio of ADN and 18C6. Various experimental measures of ADN-18C6 showed a higher melting point (151.6 °C) in comparison to pure ADN (92.6 °C), and very low hygroscopicity (0.9%, in comparison to 18% for ADN) in similar humidity conditions, along with very low impact sensitivity. However, the energetic calculation showed lower specific impulse in comparison to pure ADN. Similarly, a ADN/TANPDO (2,4,6-triamino-5-nitropyrimidine-1,3-dioxide) supramolecule crystal in the ratio 3:2 was produced using a reaction crystallization assembly method [115]. ADN/TANPDO showed excellent thermal stability with the absence of a melting process (no endothermic peak in DSC plot); it showed an exothermic peak at 215.6 °C, and had a decomposition temperature 22 °C higher than ADN. ADN/TANPDO also had greater mechanical insensitivity. The thermochemical calculation showed ADN/TANPDO had a 19.56% higher specific impulse as well as a higher combustion temperature than pure ADN.

Very few studies have been conducted for ADN in combination with materials other than Al metal powder. Comet et al. [116] reported a study on new composites primarily for detonation applications, where ADN was used as the oxidizer while red phosphorous (RP) or titanium hydride TiH_2 (TH) were used as fuels. At an equivalence ratio of 1, both the formulations exhibited heats of explosion more than 7 kJ/g (in comparison to pure ADN, 3.95 kJ/g) and detonation velocities between 1.0 and 2.0 km/s, with run of detonation distances from 20 to 40 mm for 3 mm circular tubes at around 40% of the theoretically maximum density (TMD). The ADN/RP mix showed higher sensitivities to impact and friction than the ADN/TH mix; however, both were found to have no sensitivity to electrostatic discharge. Secondary explosive PETN powder (60% TMD) and pressed PETN pellets (95% TMD) were effectively triggered by the shockwave generated by the ADN/RP and ADN/TH. According to the article, ADN-based detonating compositions can be regarded as "green" alternatives to lead-containing primary explosives. The SEM analysis showed that phosphorous particles aggregated at the surface of ADN, showing good compatibility between these materials, while some titanium hydrides penetrated ADN crystals and the rest remained as free particles. Cristilli et al. [117] experimentally investigated the effect of mechanically stimulated Al-Mg particles on the burning behaviour of ADN/HTPB at a pressure range of 4 to 13 MPa. Three levels of mechanically activated Al(spherical)-Mg(flakes) in an 80:20 ratio were used to prepare ADN/HTPB/Al-Mg composite solid propellants with a mass ratio of 66:18:16, along with individual metal propellants. NIR/IR spectra were used to determine the temperatures of the heated gases and particles. SEM and EDX (energy-dispersive X-ray) mapping were utilized to analyse the effects of mechanical activation (milling process) on the Al-Mg mix. Among the three mixes, the first was untreated, where the SEM images clearly show the difference between the Al spherical powder and Mg flakes; the second and third mixes were prepared with low- and high-intensity milling. The high-activated mix showed more homogeneous dispersion of Al-Mg than the low-activated mix. However, the burn rate measurements of composite propellants based on Al-Mg did not show much difference among the tested samples, but the measured burn rate was slightly lower for the high-activated Al-Mg than the low-activated Al-Mg mix. The pressure exponents of the examined Al-Mg-based propellants had ranges between 0.72 and 0.87, with flame temperatures lower than adiabatic. Sims et al. [118] explored ADN-based composite solid propellant for the application of boosters in hypersonic operations. The authors demonstrated that addition of fibres of AlMg5 (95% Al and 5% Mg) alloy provided significant heat transfer from the flame zone to the inner surface of the propellant, allowing modification of the burn rate of ADN-based composite solid propellant measured at pressures of 7–26 MPa. The tested fibres had dimensions of 90 μm diameter and 0.5, 1, and 3 mm lengths. The burn rates were compared with ADN/GAP (70:30), ADN/GAP/fuel, and ADN/HTPB/fuel, with ADN as 67%, GAP

or HTPB as 30%, and 3% fuel as Al powder, Al-Mg powder mix, AlMg5 alloy in powder form, or AlMg5 of three different length fibres. The burn rate followed a linear trend for all the tested compositions on a log–log scale. The AlMg5 powder did not change the burn rate significantly compared to the ADN/GAP reference case, while ADN/GAP/Al-Mg powder reduced the burn rate drastically compared to ADN/GAP without metal additives. The ADN/GAP/AlMg5 3 mm fibre length-based composite showed a burn rate almost double that of ADN/GAP, being 84 mm/s at 26.5 MPa pressure, with a pressure coefficient less than 0.5 for the three ADN/GAP/AlMg5 cases. AlMg5 1 mm fibre addition with ADN/HTPB/fuel did not change the burn rate significantly compared to the ADN/HTPB-only composition. SEM/EDX examinations and thermal conductivity measurements were used to investigate the burning process. Figure 9 compares SEM images of the burned and unburned surfaces for the ADN/GAP/AlMg5 3 mm length fibre composition. The SEM image of the unburned surface shows the fibres are surrounded by ADN particles, which can be identified by their needle shapes. In the SEM image of the burned surface, the fibres are completely exposed, along with nearby voids created by ADN decomposition. The EDX mapping (Figure 10) confirmed the results of the SEM images: the exposed AlMg5 fibres can be clearly seen (purple colour). After decomposition, nitrogen and oxygen decrease on the surface while carbon increases. The thermal conductivity measurements showed a 22% increase of ADN/GAP propellant by adding AlMg5 fibres, irrespective of the length, while adding Al/Mg powders did not change the thermal conductivity. These outcomes prove the mechanism of enhanced burn rates due to heat transfer being facilitated from the flame zone to the inside of the propellant by the used fibres. Small-scale motor tests were also conducted with 320 gm cast propellants for ADN/GAP, ADN/GAP/Al-Mg powder, and ADN/GAP/AlMg5 3 mm fibre composite solid propellants. The burn rates for the 3 mm fibre composite showed a 45% higher burn rate (of 44.08 mm/s) than the ADN/GAP propellant. However, the use of Al-Mg powder reduces the burn rate by 13% in the ADN/GAP/fuel propellant. This opposite effect from AP-based solid propellant would need further investigation.

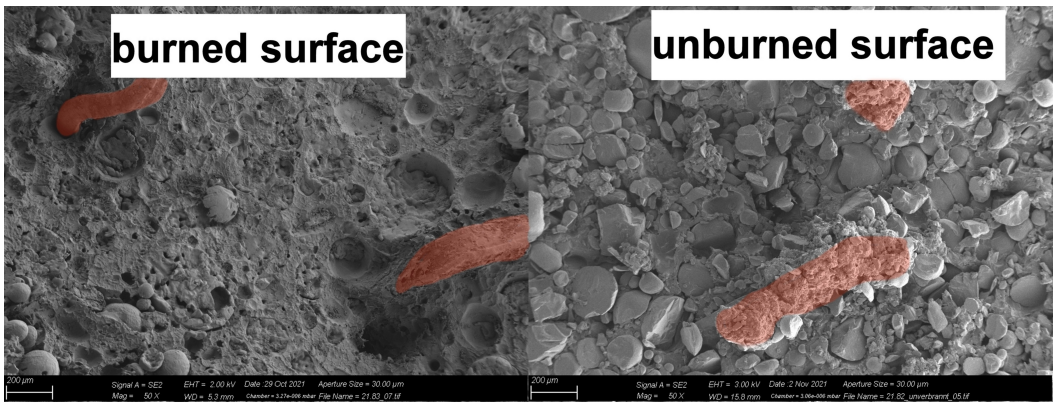

Figure 9. SEM images of ADN/GAP/AlMg5 (3 mm fibre) propellant formulations: the burned surface (**left**) and unburned surface (**right**). Fibers are spotted with red. Reproduced/adapted from [118], with permission from John Wiley and Sons.

In summary, ADN's potential as a "green" solid composite propellant with metallic fuel has been explored in the past two decades in two directions: (1) measuring the burn-rate characteristics, and (2) addressing ADN's hygroscopic nature, and mechanical and thermal sensitivities. Many experimental and theoretical studies have been conducted to estimate the burn-rate characteristics to replace AP-based traditional toxic solid propellants while exploring various compositions based on the wealth of previous knowledge and understanding of AP-based propellant combustion. Many efforts have been directed

towards obtaining required burn rates for specific applications and reducing pressure dependencies. Recently, various studies have been conducted to modify the morphology and micro-structure of ADN crystals to obtain anti-hygroscopic properties and lower the thermal and mechanical sensitivities by using various protective coatings as well as co-crystallization. However, very few studies have been performed on the burning behaviour on modified ADN surfaces and ADN co-crystal-based composite solid propellants. A very limited number of studies on the burn behaviour and physical properties of other ADN-compatible metallic fuel-based composite propellants have been conducted. Additionally, there is a very high scope for developing detailed numerical modelling and simulation tools and techniques to predict and obtain the flame structures of metallic fuel-based ADN solid composite propellants [119] and integrating them to obtain optimum compositions for various applications. There is already fundamental research going on to find suitable catalysts compatible with ADN-based liquid monopropellants [120]; however, developing and finding suitable catalysts to control the burn rate and combining them with modified morphologies/micro-structures brings more opportunities to develop ADN-based solid propellants with desired combustion performance.

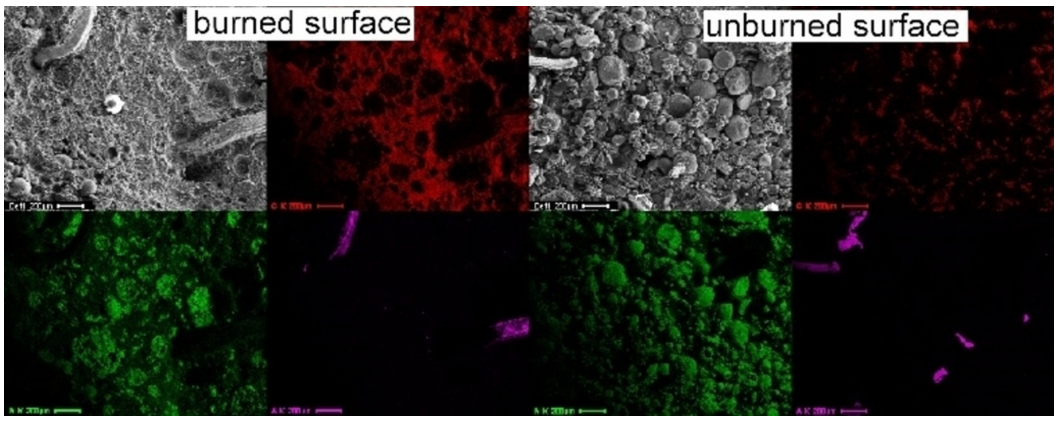

Figure 10. EDX mapping of ADN/GAP/AlMg5 (3 mm fibre) compositions; reproduced/adapted from [118], with permission from John Wiley and Sons.

6. Discussion and Future Outlook

The development of a new environmentally friendly composite solid propellant for propulsion applications and bringing its maturity up to operational level is a complex process which can expand into multiple major science and engineering research domains. It may require future sustained collaborative efforts from academic researchers, space agencies, and defence and commercial space industries to further realize a "green" rocket propellant for future multi-stage launch systems, booster, or microlauncher applications, which can also enhance reusability. The development of ADN-based "green" composite solid propellant is an emerging technology; at the current time, it can be considered at stage 4 of Gartner's hype cycle [121]. The "technology trigger" (stage 1) was started after ADN's discovery in 1971 and its re-invention and public knowledge in 1988, owing to its high performance and ecological benefits. With the "peak of inflated expectation" (stage 2) of replacing the already-existing mature AP-based solid propellant for launch vehicles, sustained efforts have been made for developing ADN-based composite solid propellant from the 1990s to the last decade, especially in Europe. Various combinations of ADN-based composite solid propellants were developed, the propellant fabrication processes were adapted, and testing campaigns were conducted to measure and estimate their ballistic properties, along with lab-scale rocket motor testing. However, a slight "trough of disillusionment" (stage 3) was observed when the challenges associated with ADN-based solid

propellant were realized, including obtaining target burn rates and its pressure dependency for specific applications, its hygroscopic nature, and its high sensitivity to mechanical and thermal loads, which lead to issues in handling, long-term storage, and transport. As mentioned, the development cycle of ADN-based solid propellant is now in stage 4, which is termed the "slope of enlightenment", when many technologies and processes are being developed to modify the micro-structural and morphological properties of ADN-based formulations to achieve mechanical and thermal stability and anti-hygroscopic properties, as well as balancing the burn properties of green solid propellants. Future sustained research efforts will be further required to realize the "plateau of productivity" as the final stage (stage 5) to achieve operational ADN-based green solid propellant in many space applications. The main challenges in developing viable ADN-based solid propellant lie in formulating a suitable composite with low hygroscopicity, enhanced thermal, mechanical, and chemical stability, and the ability to deliver the required burning performance while ensuring operational viability during rocket motor tests and actual launches. Previous researchers have explored various theoretical, experimental, and numerical techniques to support the development of ADN-based solid propellant up to now, which further require advancement also. Based on existing tools and techniques and future advancements, the authors would like to discuss the following possible pathways for future research to realize an efficient and desirable ADN-based green solid propellant.

6.1. Pathway 1: Quantum Chemistry and Molecular Thermodynamics

ADN-based composite solid propellants can have many organic, non-organic, and metallic ingredients, with ADN as the oxidizer (mono-modal or bi-modal), and then a binder (energetic/non-energetic), plasticizer, energetic fuel (metallic/non-metallic), curing agent, stabilizer, catalyst. Up to now, many studies have explored/developed ADN-based solid propellant based on previous knowledge and understanding of AP-based or AP-compatible ingredients. It may be required to explore existing or new ingredients and their compatibility in a systematic manner, especially with ADN. Hahma et al. [122] highlight ADN's incompatibility with many materials and impurities, which either react with ADN or catalyse the decomposition of ADN or both. Some totally incompatible materials are iron, nickel, copper, silver and its alloys and compounds, cyanoacrylate glue, and polyacetal (Delrin). Some of these can cause autoignition of ADN, even with molten ADN. The compatible materials are stainless steel (SS2343, V4A, AISI316), aluminium, magnesium, gold, polytetrafluoro-ethylene (PTFE), perfluorinated rubber (Viton), polyethylene without dyestuffs, RDX, HMX, zinc oxide, magnesium oxide, Dow Sylgard 170 two-component silicone resin, and plexiglass (as thoroughly cured polymer only). In order to evaluate the compatibility with various substances, quantum chemistry and molecular thermodynamics-based calculations can be employed along with relevant testing. Very few studies have applied these methods to ADN. Rahm [123,124] has theoretically investigated the kinetic stability, reactivity, and solid-state behaviour of possible green energetic materials (GEMs) in the gaseous state and in a low polarity solvent (THF) by analysing various possible decomposition pathways for each compound. Along with ADN, the study proposed new oxygen- and nitrogen-rich compounds, which can have high energy content as well as a high oxygen balance. Both these properties lead to better performance while reducing the requirement for metallic fuel. A lesser amount of metallic fuel can lead to a reduced combustion temperature and reduced smoke formation, as well as being lighter and having cheaper fabrication. Several material properties such as density, solid-state heat of formation, and propellant performance were estimated with theoretical calculations. Isocyanate curing agents are toxic to humans, as well as incompatible with ADN. The study also explored compatible curing agents based on poly-oxetanes for ADN/GAP-based composite

propellant. Ren et al. [125] and Zheng et al. [126] have employed molecular simulations to tune the hygroscopic nature of ADN with several energetic materials as co-crystal ligands of ADN. Lu et al. [127] have summarized various studies on the simulation of ADN based on density functional theory (DFT), molecular dynamics (MD) calculations, the Monte Carlo (MC) method, and other numerical simulations. The quantum chemical and microscopic molecular dynamics models can reveal the relationship between the molecular structure and macroscopic thermal and material properties. The prediction of ageing and degradation of thermal and mechanical properties of composite solid propellant over time (usually decades) under storage conditions is another important direction to advance composite solid propellant technology. Accelerated ageing techniques are used to experimentally evaluate the ageing process; this may not reliably predict the degradation process on actual timescales. Multiscale quantum chemical and molecular dynamics models are required to overcome the shortcomings of experimental methods and can be used to predict the degradation mechanism and rates, and the impact of the interface and material properties as a function of time. Further, the solid-phase behaviour under mechanical and thermal loading can be analysed by adapting mesoscopic and macroscopic modelling [128] for ADN-based composite propellants. Recently, Kumar et al. [129] have presented a numerical framework to investigate the thermo-mechanical deformation of burning heterogeneous solid propellant by using coupled solid–gas-phase models. Thermal and mechanical loading can also result in forming voids; the mechanisms of forming micro-voids and microcracks and their evolution or debonding within composite solid propellants can also be investigated; they are responsible for promoting uneven burn, leading to potential failure upon use. Based on the finding of a compatible formulation, suitable manufacturing processes can be explored for ADN-based composite solid propellants for long-term storage, and effective transport and handling, along with the desired energetic performance.

6.2. Pathway 2: ADN with Various Metallic Fuels

The combustion of ADN composites with metallic fuel results in a highly energetic reaction, generating hot gases that are expelled through a nozzle, producing thrust and propelling the rocket. The combustion performance of ADN composite solid propellant can be influenced by various factors, including particle size and distribution, mixing ratio with the fuel, pressure, and temperature conditions. Scientists and engineers continuously study and optimize these factors to maximize the efficiency and stability of ADN-based propulsion systems. Furthermore, the combustion characteristics of ADN can also be tailored by the addition of suitable additives, catalysts, or binders to control the burn rate, ignition sensitivity, and overall performance. This allows the customization of ADN-based propellants to meet specific requirements and applications. The previous studies on ADN-based composite solid propellants mainly focused on using aluminium as metallic fuel in the form of micro-sized (μAl), nano-sized (n-Al), or activated (act-Al) Al in various compositions. However, there are very few studies focused on other metallic fuels such as magnesium (Mg) or aluminium hydrides and titanium hydrides, while there are no studies on other metallic fuels such as titanium (Ti), zirconium (Zr), metalloid fuel boron (B), or different powder mixes or compounds to control the burn performance of ADN-based solid propellants. The burn rates at various operating pressures and the pressure sensitivities have mainly been measured and computed using a Crawford/strand burner with optical access. Many studies have employed thermocouple-based and optical temperature measurements as well as spectrometric analysis to predict the spatial and temporal temperature and species variations and to identify various kinetics. Various types of SEM/XRD and other surface morphology and micro-structure identification techniques have also been integrated for pre-, post-, or in situ combustion analysis. Only a few studies have em-

ployed lab-scale rocket motor testing. Metal combustion in oxygen/air is a challenging research area itself, and metal combustion in the presence of various oxidizers, binders, and other additives leads to more challenges. However, it is recommended to focus on understanding the metal combustion phenomenon by combining experimental and numerical modelling and simulation tools for metal ignition, the effect of condensed products and the aggregation/agglomeration phenomenon on metal combustion, the kinetics of combustion, the influence of various factors of metal combustion on propellant burning, estimation of two-phase loss, slag formation, the impact of the presence of additives, and the use of metal alloys. Experimental methods such as SEM/XRD can be employed in pre- and post-combustion of single- or multi-particle combustion stages. The use of metal filaments and catalysts can also be explored for burn-rate measurements and understanding the mechanism for burn-rate modification. New technologies to control the burn characteristics of metal-based solid propellants can be adapted, as studied by Wen et al. [130], who used a DC electric field to move metallic particles in the flame towards the burning surface. The studies on kinetically controlled combustion and diffusion-controlled combustion in metallic solid propellant and their transition from one to another can also be explored to adapt burn-rate requirements with suitable mono-modal or bi-modal oxidizers, binders, plasticizers, catalysts, and stabilizers.

6.3. Pathway 3: Composite Propellants with Modified ADN Surfaces and Crystals

Recent studies [10,112–115] have explored various fabrication processes to modify the surface morphology by protective coatings and combining additional compounds with ADN to produce supramolecules with co-crystallization. These surface and crystal modifications of ADN can overcome the stability and sensitivity challenges of pure ADN, developing compounds with higher melting points, low mechanical sensitivities, and low hygroscopicity compared to pure ADN. Thermal stability is evaluated using differential scanning calorimetry (DSC) and thermogravimetry analysis (TGA), while impact and friction sensitivities are estimated using BAM friction and sensitivity tests. SEM/XRD/EDS have also been used for analysis of micro-structure, morphology, and elemental maps of ADN's reactant, intermediate, and final combustion products. The hygroscopic rates were also measured for the modified samples, along with pure ADN. In many of these studies, the energetic performance was obtained by either simplified numerical calculations or qualitative visualization. It is expected these new formulations, with enhanced properties for ADN, will be utilized for composite propellant formation in the future and burn-rate characteristics will be used to assess their performance with all ingredients, along with the modified ADN. It will also be interesting to know whether these new compounds of ADN retain their properties when used for larger-size composite propellant formation processes. Molecular dynamics simulations and quantum chemical simulations can pave the way to identify many more modified ADN oxidizers and composite propellants, which can be tailored to the desired energetic performance with significantly enhanced stability properties.

6.4. Pathway 4: ADN Composite Flame Modelling

The flame structure of ADN-based composite solid propellant can be complex due to various fluid, thermodynamic, chemical, and heat transfer mechanisms involved in multiphase zones at various temporal and spatial scales. Initially, many studies utilized equilibrium chemistry as well as 1D modelling to obtain the ADN-monopropellant flame structure. Thakre et al. [76] modelled ADN combustion using coupled condensed- and gas-phase models with finite-rate chemical kinetics. Generally, the combustion modelling of solid propellant requires considering the solid-phase heat transfer modelling, foam

layer (consisting of solid bubbles or liquid bubbles) modelling, and gas-phase kinetics to predict the flame structure and burn rate. Many simple and complex techniques are used to link the condensed phase and gas phase in 1D modelling, such as (1) assuming condensed-phase decomposition with simplified Arrhenius equations and energy conservation equations, (2) modelling condensed-phase decomposition with semi-global kinetic mechanisms, and (3) modelling the receding surface along with mass, momentum, energy, and species conservation. In two-dimensions, sandwich modelling [79,131] has been adapted by various researchers for composite solid propellant with oxidizer and binder mixtures, keeping one at the centre and the other on both sides, without metallic fuels. The inlet boundary conditions for these models are obtained by mass and heat flux continuity at the vaporizing surface along with considering pyrolysis laws. The simulations can use simplified chemistry to provide burn rate predictions close to experimental data. The basic flame structure in the gas phase can be obtained for non-aluminized combustion of oxidizer and binders. It consists of a primary flame from the reacting oxidizer and binder; a premixed oxidizer flame; and a final diffusion flame, involving products of the other two flames. However, detailed chemical kinetics are often required to accurately predict the detailed flame structures and interactions, species mass/mole fractions, and the rate of production and consumption of intermediates and reaction products. If multiple ingredients are modelled, their detailed chemical kinetics should be optimized for the mixture's components. Kore et al. [119] studied the impact of adding Al to an ADN/HTPB formulation and obtained a diffusion flame with a dark zone for ADN/HTPB, which came closer to surface and reduced the dark zone with the addition of Al. The development of ADN-based composite propellant can be accelerated if the numerical simulation methods are integrated with experimental measurements, which would require modelling various thermochemical processes in flame formation. This modelling and simulation will not be possible without focused development of detailed chemical kinetics for reactants in composite solid propellant, and their integration as well as validation. There is a further requirement to develop integrated models for metallic fuel combustion in the presence of an oxidizer and binder flame, develop am understanding of surface reactions, and predict the agglomeration phenomenon and two-phase flow losses. The prediction of flame formation, temperature distribution, and an analysis of the formation of various reactions and major and minor reaction products can provide greater insight into combustion behaviour and the impact of various uncertainties in propellant performance, allowing a significant reduction in the number of experimental trials for future development of ADN-based "green" solid propellant.

6.5. Pathway 5: Small- and Full-Scale Solid Motor Testing

In the early development phases of new solid propellant, burn-rate measurements using small sample sizes through a strand burner play an important role in optimizing the composition and formulation of various ingredients. The burn rate, with burning area, determines the combustion processes and the mass flow rate, and therefore directly controls the pressure and thrust of the motor. The propellant burns in one-dimension in a strand burner with small sample sizes, which can decouple the burn rate from other phenomena present in the motor. Hence, the burn rate measured in a strand burner can be different than in actual motor firing, usually lower than motor testing. The higher motor burning rate can be caused by a difference in sample size, preparation methods, cross-flow velocities, higher heat transfer, unstable combustion, presence of cracks or voids in the grain, etc. Hence, it is important to develop a correlation, the "burn-rate scale factor", between burn rates measured in a strand burner and actual motor testing [132]. Due to the high cost of performing full-scale motor tests, small-scale (200 gms–5 kg) or large sub-scale (5–10 kg)

motor testing are integrated in propellant development and optimizing operations by estimating different burn-rate scale factors. Additionally, rocket motor testing can provide knowledge and understanding of the pressure and thrust vs. time history, the effectiveness of the case insulation, the nozzle throat erosion, the effect of a prior environmental treatment on the internal ballistics, and the operation of a thrust vector control mechanism or thrust cut-off device, and the structural integrity of the propellant grain, developing the various compatible systems and their integration towards practical usability. After determining or identifying the possible combinations of ADN-based green solid propellants, small-scale motor testing would pave the way for future integration and up-scaling of a new green solid propellant. Lab-scale testing related to motor size, performance, and burn time will provide knowledge of its usefulness towards actual operations. Later, full motor testing will finally provide an opportunity for development of operations towards launching integration of ADN-based green solid propellants.

7. Conclusions

Globally, the space launch market size is growing rapidly [133]. In the current decade, every year 4000–5000 satellite launches are projected, due to growing commercial interests in a variety of applications: weather monitoring, surveillance, Earth observation, navigation, communication, meteorology, and more [134]. Additionally, the advances in reusable rockets and small-satellite technologies is fuelling the demand for low-cost, flexible, safe, and reliable on-demand microlaunch vehicles for sustainable growth [134,135]. To realize the projected growth trajectory in a sustainable manner, it is required to develop rocket-launch and space-propulsion systems with propellants which are environmentally friendly as well as non-toxic, while being able to be handled, stored, and transported for rapid deployment. ADN is considered one of the most promising choices for green solid propulsion systems due to its excellent ballistic properties. The ability to harness the combined energy output of ADN and metal/metalloid fuels or various emerging compounds/combinations could enable more efficient satellite launches, prolonged mission durations, and increased manoeuvrability of spacecraft. The development of ADN-based green solid propellant has been in progress for the past two decades. Along with its good performance characteristics of a higher burn rate, high heat of formation, and higher specific impulse, there are a few challenges to address before its more mature application in microlaunchers, first-stage or second-stage space propulsion, or boosters, such as its thermal and mechanical stabilities, compatibility with different materials, hygroscopic nature, and controlling the burn rate for specific applications. This comprehensive literature review, with a focus on the combustion behaviour of ADN-based green solid propellants with metal additives, provides information and understanding on the comparative physiochemical properties of ADN, its thermal decomposition mechanism, the combustion behaviour of ADN and techniques used to understand it, the combustion behaviour of ADN with metal additives and the impact of various techniques to tailor its performance, thermal and mechanical stability, and to overcome its hygroscopic nature. Finally, the possible future research pathways are identified and discussed for rapid accelerated development of ADN-based green solid propellant as a viable solution for future propulsion applications.

Author Contributions: Conceptualization, R.K.; methodology, R.K.; formal analysis, R.K. and A.V.; investigation, R.K.; resources, R.K. and A.V.; data curation, R.K.; writing—original draft preparation, R.K.; writing—review and editing, A.V.; supervision, A.V.; project administration, A.V.; funding acquisition, R.K. and A.V. All authors have read and agreed to the published version of the manuscript.

Funding: This research was funded by Government of Ireland Postgraduate Scholarship Programme, grant number GOIPG/2022/1806 by Irish Research Council (Research Ireland). The Open Access publication cost is supported by Research Connexions Program 2024: Open-Access Pathway 6 by South East Technological University.

Institutional Review Board Statement: Not applicable.

Informed Consent Statement: Not applicable.

Data Availability Statement: Not applicable.

Conflicts of Interest: The authors declare no conflicts of interest.

References

1. Bottaro, J.C.; Penwell, P.E.; Schmitt, R.J. 1,1,3,3-Tetraoxo-1,2,3-triazapropene Anion, a New Oxy Anion of Nitrogen: The Dinitramide Anion and Its Salts. *J. Am. Chem. Soc.* **1997**, *119*, 9405–9410. [CrossRef]
2. Luk'yanov, O.A.; Gorelik, V.P.; Tartakovskii, V.A. Dinitramide and its salts. *Russ. Chem. Bull.* **1994**, *43*, 89–92. [CrossRef]
3. Brill, T.B.; Ren, W.Z.; Yang, V., Synthesis and Characterization of Dinitramidic Acid and Its Salts. In *Solid Propellant Chemistry, Combustion, and Motor Interior Ballistics*; AIAA: Reston, VA, USA , 2000; Chapter 1.8, pp. 207–220. [CrossRef]
4. Talawar, M.B.; Sivabalan, R.; Anniyappan, M.; Gore, G.; S.N., A.; Gandhe, B.R. Emerging trends in advanced high energy materials. *Combust. Explos. Shock Waves* **2007**, *43*, 62–72. [CrossRef]
5. Larsson, A.; Wingborg, N. Green Propellants Based on Ammonium Dinitramide (ADN). In *Advances in Spacecraft Technologies*; Hall, J., Ed.; IntechOpen: Rijeka, Croatia, 2011; Chapter 7. [CrossRef]
6. Venkatachalam, S.; Santhosh, G.; Ninan Ninan, K. An Overview on the Synthetic Routes and Properties of Ammonium Dinitramide (ADN) and other Dinitramide Salts. *Propellants, Explos. Pyrotech.* **2004**, *29*, 178–187. [CrossRef]
7. Touidjine, S.; Karim Boulkadid, M.; Trache, D.; Belkhiri, S.; Mezroua, A.; Islam Aleg, M.; Belkebiche, A. Preparation of ammonium nitrate-based solid composite propellants supplemented with polyurethane/nitrocellulose blends binder and their thermal decomposition behavior. *Def. Technol.* **2022**, *18*, 2023–2033. [CrossRef]
8. Kubota, N., Energetics of Propellants and Explosives. In *Propellants and Explosives*; John Wiley & Sons, Ltd: Hoboken, NJ, USA, 2015; Chapter 4, pp. 73–117. [CrossRef]
9. Agrawal, J.P.; Walley, S.M.; Field, J.E. High-Speed Photographic Study of the Impact Response of Ammonium Dinitramide and Glycidyl Azide Polymer. *J. Propuls. Power* **1997**, *13*, 463–470. [CrossRef]
10. Yang, H.; Chen, F.; Hu, Y.; Lu, Q.; Xiao, L.; Wang, Y.; Zhao, F.; Jiang, W.; Hao, G. A review on surface coating strategies for anti-hygroscopic of high energy oxidizer ammonium dinitramide. *Def. Technol.* **2024**, *33*, 237–269. [CrossRef]
11. Bellas, M.K.; Matzger, A.J. Achieving Balanced Energetics through Cocrystallization. *Angew. Chem. Int. Ed.* **2019**, *58*, 17185–17188. [CrossRef]
12. De Flon, J.; Andreasson, S.; Liljedahl, M.; Oscarson, C.; Wanhatalo, M.; Wingborg, N., Solid Propellants based on ADN and HTPB. In Proceedings of the 47th AIAA/ASME/SAE/ASEE Joint Propulsion Conference & Exhibit, AIAA-2011-6136, San Diego, California, USA, 31 July–3 August 2011 ; pp. 1–12. [CrossRef]
13. Nair, U.; Asthana, S.; Rao, A.; Gandhe, B. Advances in High Energy Materials (Review Paper). *Def. Sci. J.* **2010**, *60*, 137–151. [CrossRef]
14. Weiser, V.; Eisenreich, N.; Baier, A.; Eckl, W. Burning Behaviour of ADN Formulations. *Propellants Explos. Pyrotech.* **1999**, *24*, 163–167. :03<163::AID-PREP163>3.0.CO;2-K [CrossRef]
15. Landsem, E.; Jensen, T.L.; Hansen, F.K.; Unneberg, E.; Kristensen, T.E. Mechanical Properties of Smokeless Composite Rocket Propellants Based on Prilled Ammonium Dinitramide. *Propellants Explos. Pyrotech.* **2012**, *37*, 691–698. [CrossRef]
16. Chakravarthy, S.R.; Freeman, J.M.; Price, E.W.; Sigman, R.K. Combustion of Propellants with Ammonium Dinitramide. *Propellants Explos. Pyrotech.* **2004**, *29*, 220–230. [CrossRef]
17. Harimech, Z.; Toshtay, K.; Atamanov, M.; Azat, S.; Amrousse, R. Thermal Decomposition of Ammonium Dinitramide (ADN) as Green Energy Source for Space Propulsion. *Aerospace* **2023**, *10*, 832. [CrossRef]
18. Friedhoff, P.; Anflo, K.; Thormahlen, P.; Persson, M., Growing Constellation of Ammonium Dinitramide (ADN) Based High Performance Green Propulsion (HPGP) Systems. In Proceedings of the 2018 Joint Propulsion Conference, AIAA-2018-4754, Cincinnati, Ohio, USA, 9–11 July 2018; pp. 1–9. [CrossRef]
19. Heintz, T.; Leisinger, K.; Reinhardt, W.; Heil, M.; Herrmann, M. Product design of ADN-PRILLS for applications in solid propellants. In Proceedings of the Fraunhofer-Institut für Chemische Technologie (International Annual Conference), Karlsruhe, 26-29 June 2018. [CrossRef]
20. Wingborg, N. Ammonium Dinitramide—Water: Interaction and Properties. *J. Chem. Eng. Data* **2006**, *51*, 1582–1586. [CrossRef]

21. Chen, F.; Xuan, C.; Lu, Q.; Xiao, L.; Yang, J.; Hu, Y.; Zhang, G.; Wang, Y.; Zhao, F.; Hao, G.; et al. A review on the high energy oxidizer ammonium dinitramide: Its synthesis, thermal decomposition, hygroscopicity, and application in energetic materials. *Def. Technol.* **2023**, *19*, 163–195. [CrossRef]
22. Wang, W. Advances and prospects of energetic material technologies. *J. Solid Rocket. Technol.* **2003**, *26*, 42–8. [CrossRef]
23. Ostmark, H.; Bemm, U.; Langlet, A.; Sanden, R.; Wingborg, N. The properties of ammonium dinitramide (ADN): Part 1, basic properties and spectroscopic data. *J. Energetic Mater.* **2000**, *18*, 123–138. [CrossRef]
24. Zhao, X.; Hou, L.F.; Zhang, X.P. High Performance Propellant Oxidizer Nitoformhydrazine (HNF). *Aerodyn. Missile J.* **1998**, *7*, 30–32. [CrossRef]
25. Zheng, J.; Hou, L.; Yang, Z. The progress and prospects of high energy propellants. *J. Solid Rocket. Technol.* **2001**, *24*, 28–34. [CrossRef]
26. Langlet, A.; Wingborg, N.; Ostmark, H. ADN: A new high performance oxidizer for solid propellants. *Int. J. Energetic Mater. Chem. Propuls.* **1997**, *4*, 616–626. [CrossRef]
27. Zhang, Z.; Wang, B.; Ji, Y.; Zhou, Y.; Zhou, C.; Liu, Q.; Zhu, C. Study progress of several high energy density materials (HEDM). *Chin. J. Explos. Propellants* **2008**, *31*, 93–7. [CrossRef]
28. Yang, R.; Thakre, P.; Yang, V. Thermal Decomposition and Combustion of Ammonium Dinitramide (Review). *Combust. Explos. Shock Waves* **2005**, *41*, 657–679. [CrossRef]
29. Cardao, P.A.; Gois, J.C.; Campos, J.A. Thermal decomposition of energetic materials. *AIP Conf. Proc.* **2000**, *505*, 853–856. [CrossRef]
30. Golofit, T.; Zysk, K. Thermal decomposition properties and compatibility of CL-20 with binders HTPB, PBAN, GAP and polyNIMMO. *J. Therm. Anal. Calorim.* **2015**, *119*, 1931–1939. [CrossRef]
31. Sun, X.; Wang, J.; Zhou, X.L. Thermal decomposition kinetics and thermal safety of HNF. *Hanneng Cailiao/Chinese J. Energetic Mater.* **2014**, *22*, 774–779. [CrossRef]
32. Kumar, P. An overview on properties, thermal decomposition, and combustion behavior of ADN and ADN based solid propellants. *Def. Technol.* **2018**, *14*, 661–673. [CrossRef]
33. Fan, X.P.; Wang, X.; Liu, Z.; Huimin, T. Catalysis of nano Cu powder on the thermal decomposition of HMX and RDX. *Hanneng Cailiao/Chinese J. Energetic Mater.* **2005**, *13*, 284–7. [CrossRef]
34. Kinkead, E.; Salin, S.; Wolfe, R. Acute and Subacute Toxicity Evaluation of Ammonium Dinitramide. Technical Report AL/OE-TR-1994-0071, Mantech Environmental Technology, Dayton, OH 45437-0009, USA, 1994. Available online: https://apps.dtic.mil/sti/tr/pdf/ADA298965.pdf (accessed on 31 December, 2024).
35. Rossi, M.J.; Bottaro, J.C.; McMillen, D.F. The thermal decomposition of the new energetic material ammonium dinitramide ($NH_4N(NO_2)_2$) in relation to Nitramide (NH_2NO_2) and NH_4NO_3. *Int. J. Chem. Kinet.* **1993**, *25*, 549–570. [CrossRef]
36. Brill, T.; Brush, P.; Patil, D. Thermal decomposition of energetic materials 58. Chemistry of ammonium nitrate and ammonium dinitramide near the burning surface temperature. *Combust. Flame* **1993**, *92*, 178–186. [CrossRef]
37. Oxley, J.C.; Smith, J.L.; Zheng, W.; Rogers, E.; Coburn, M.D. Thermal Decomposition Studies on Ammonium Dinitramide (ADN) and 15N and 2H Isotopomers. *J. Phys. Chem. A* **1997**, *101*, 5646–5652. [CrossRef]
38. Lobbecke, S.; Keicher, T.; Krause, H.; Pfeil, A. The new energetic material ammonium dinitramide and its thermal decomposition. *Solid State Ionics* **1997**, *101-103*, 945–951. International Symposium on the Reactivity of Solids, [CrossRef]
39. Vyazovkin, S.; Wight, C.A. Thermal Decomposition of Ammonium Dinitramide at Moderate and High Temperatures. *J. Phys. Chem. A* **1997**, *101*, 7217–7221. [CrossRef]
40. Fetherolf, B.; Litzinger, T. CO_2 Laser-Induced Combustion of Ammonium Dinitramide (ADN). *Combust. Flame* **1998**, *114*, 515–530. [CrossRef]
41. Park, J.; Chakraborty, D.; Lin, M. Thermal decomposition of gaseous ammonium dinitramide at low pressure: Kinetic modeling of product formation with ab initio MO/cVRRKM calculations. *Symp. (Int.) Combust.* **1998**, *27*, 2351–2357. [CrossRef]
42. Ermolin, N. Modeling of Pyrolysis of Ammonium Dinitramide Sublimation Products under Lower Pressure Conditions. *Combust. Explos. Shock Waves* **2004**, *40*, 92–109. :CESW.0000013672.66809.32 [CrossRef]
43. Shmakov, A.; Korobeinichev, O.; Bol'shova, T. Thermal Decomposition of Ammonium Dinitramide Vapor in a Two-Temperature Flow Reactor. *Combust. Explos. Shock Waves* **2002**, *38*, 284–294. :1015697618376 [CrossRef]
44. Santhosh, G.; Ghee, A. Synthesis and kinetic analysis of isothermal and non-isothermal decomposition of ammonium dinitramide prills. *J. Therm. Anal. Calorim.* **2008**, *94*, 263–270. [CrossRef]
45. Matsunaga, H.; Habu, H.; Miyake, A. Thermal behavior of new oxidizer ammonium dinitramide. *J. Therm. Anal. Calorim.* **2013**, *111*, 1183–1188. [CrossRef]
46. Andreev, A.; Anikin, O.; Ivanov, A.; Krylov, V.K.; Pak, Z.P. Stabilization of ammonium dinitramide in the liquid phase. *Russ. Chem. Bull.* **2000**, *49*, 1974–1976. :1009555405171 [CrossRef]
47. Mishra, I.B.; Russell, T. Thermal stability of ammonium dinitramide. *Thermochim. Acta* **2002**, *384*, 47–56. [CrossRef]
48. Pavlov, A.N. Decomposition mechanism of dinitramide onium salts. *Russ. Chem. Bull.* **1997**, *46*, 1848–1850. [CrossRef]

49. Lobbecke, S.; Krause, H.H.; Pfeil, A. Thermal Analysis of Ammonium Dinitramide Decomposition. *Propellants Explos. Pyrotech.* **1997**, *22*, 184–188. [CrossRef]
50. Vyazovkin, S.; Wight, C.A. Ammonium Dinitramide: Kinetics and Mechanism of Thermal Decomposition. *J. Phys. Chem. A* **1997**, *101*, 5653–5658. [CrossRef]
51. Kazakov, A.I.; Rubtsov, Y.I.; Andrienko, L.P.; Manelis, G.B. Kinetics of the thermal decomposition of dinitramide: 3. Kinetics of the heat release during the thermal decomposition of dinitramide ammonium salt in the liquid phase. *Phys. Chem.* **1998**, *47*, 379–385. [CrossRef]
52. Manelis, G.B. Thermal Decomposition of Dinitramide Salt. In Proceedings of the 26th International Annual Conference of ICT, Pyrotechnics—Basic Principles, Technology, Application, FRG, Karlsruhe, Germany, 4–7 July 1995; pp. 15.1–15.17.
53. Pavlov, A.N.; Grebennikov, V.N.; Nazina, L.D.; M., N.G.; B., M.G. Thermal decomposition of ammonium dinitramide and mechanism of anomalous decay of dinitramide salts. *Russ. Chem. Bull.* **1999**, *48*, 50–54. [CrossRef]
54. Ermolin, N.; Fomin, V. On the mechanism of thermal decomposition of ammonium dinitramide (review). *Combust. Explos. Shock Waves* **2016**, *52*, 566–586. [CrossRef]
55. Politzer, P.; Seminario, J.M.; Concha, M.C. Energetics of ammonium dinitramide decomposition steps. *J. Mol. Struct. THEOCHEM* **1998**, *427*, 123–129. [CrossRef]
56. Beckstead, M., An overview of combustion mechanisms and flame structures for advanced solid propellants. In Proceedings of the 36th AIAA/ASME/SAE/ASEE Joint Propulsion Conference and Exhibit, AIAA-2000-3325, Las Vegas, NV, USA, 24–28 July2000; pp. 1–17. [CrossRef]
57. Pak, Z., Some ways to higher environmental safety of solid rocket propellant application. In Proceedings of the 29th Joint Propulsion Conference and Exhibit, AIAA-93-1755, Monterey, CA, USA, 28–30 June 1993; pp. 1–6. [CrossRef]
58. Merzhanov, A. The theory of stable homogeneous combustion of condensed substances. *Combust. Flame* **1969**, *13*, 143–156. [CrossRef]
59. Atwood, A.I.; Boggs, T.L.; Curran, P.O.; Parr, T.P.; Hanson-Parr, D.M.; Price, C.F.; Wiknich, J. Burning Rate of Solid Propellant Ingredients, Part 1: Pressure and Initial Temperature Effects. *J. Propuls. Power* **1999**, *15*, 740–747. [CrossRef]
60. Atwood, A.I.; Boggs, T.L.; Curran, P.O.; Parr, T.P.; Hanson-Parr, D.M.; Price, C.F.; Wiknich, J. Burning Rate of Solid Propellant Ingredients, Part 2: Determination of Burning Rate Temperature Sensitivity. *J. Propuls. Power* **1999**, *15*, 748–752. [CrossRef]
61. Korobeinichev, O.; Kuibida, L.; Paletsky, A.; A.G., S., Study of Flame Structure, Kinetics and Mechanism of the Thermal Decompostion of Solid Propellant by probing Mass Spectrometry. In *Challenges in Propellants and Combustion: 100 Years After Nobel*; Begell House: Danbury, CT, USA, 1997; pp. 38–47.
62. Korobeinichev, O.; Kuibida, L.; Paletsky, A.; Shmakov, A., Development and application of molecular beam mass-spectrometry to the study of ADN combustion chemistry. In Proceedings of the 36th AIAA Aerospace Sciences Meeting and Exhibit, AIAA-98-0445, Reno, NV, USA, 12–15 January1998; pp. 1–14. [CrossRef]
63. Strunin, V.; Dyakov, A.; Manelis, G. Combustion of ammonium dinitramide. *Combust. Flame* **1999**, *117*, 429–434. [CrossRef]
64. Zenin, A.; Puchkov, V.; Finjakov, S., Physics of ADN combustion. In Proceedings of the 37th Aerospace Sciences Meeting and Exhibit, AIAA-99-595, Reno, NV, USA, 11–14 January1999; pp. 1–10. [CrossRef]
65. Ermolin, N. Heat-release mechanism in ammonium dinitramide flame. *Combust. Explos. Shock Waves* **2006**, *43*, 549–561. [CrossRef]
66. Korobeinichev, O.P.; Kuibida, L.V.; Paletsky, A.A.; Shmakov, A.G. Molecular-Beam Mass-Spectrometry to Ammonium Dinitramide Combustion Chemistry Studies. *J. Propuls. Power* **1998**, *14*, 991–1000. [CrossRef]
67. Rossi, M.; McMillen, D.; Golden, D. Low Pressure Thermal Decomposition Studies Selected Nitramine and Dinitramine Energetic Materials. Technical Report DTIC ADA247972, Defense Technical Information Center, SRI Project 8999, Fort Belvoir, VA, USA, 1992.
68. Fogelzang, A.; Stinditskii, V.; Egroshev, V.; Levshenkov, A.; Serushkin, V.; Kolesov, V. Combustion behavior and flame structure of ammonium dinitramide. In Proceedings of the 28th International Annual Conference of ICT, FRG, Karlsruhe, Germany, 25-28June 1997; pp. 1–14.
69. Korobeinichev, O.P.; Bolshova, T.A.; Paletsky, A.A. Modeling the chemical reactions of ammonium dinitramide (ADN) in a flame. *Combust. Flame* **2001**, *126*, 1516–1523. [CrossRef]
70. Ramaswamy, A. Energetic-material combustion experiments on propellant formulations containing prilled ammonium dinitramide. *Combust. Explos. Shock Waves* **2000**, *36*, 119–124. [CrossRef]
71. Ramaswamy, A.L. Study of the thermal initiation of ammonium dinitramide (ADN) crystals and prills. *J. Energetic Mater.* **2000**, *18*, 39–60. [CrossRef]
72. Sinditskii, V.P.; Egorshev, V.Y.; Levshenkov, A.I.; Serushkin, V.V. Combustion of Ammonium Dinitramide, Part I: Burning Behavior. *J. Propuls. Power* **2006**, *22*, 769–776. [CrossRef]
73. Sinditskii, V.P.; Egorshev, V.Y.; Levshenkov, A.I.; Serushkin, V. Combustion of Ammonium Dinitramide, Part 2: Combustion Mechanism. *J. Propuls. Power* **2006**, *22*, 777–785. [CrossRef]

74. Sinditskii, V.P.; Egorshev, V.Y.; Serushkin, V.V.; Filatov, S.A. Combustion of energetic materials controlled by condensed-phase reactions. *Combust. Explos. Shock Waves* **2012**, *48*, 81–99. [CrossRef]
75. Gross, M.L. Two-Dimensional Modeling of AP/HTPB Utilizing a Vorticity Formulation and One-Dimensional Modeling of AP and ADN. Ph.D. Thesis . 1167, Brigham Young University, Provo, UT, USA, 2007. Available online: https://scholarsarchive.byu.edu/etd/1167/ (accessed on)31 December 2024.
76. Thakre, P.; Duan, Y.; Yang, V. Modeling of ammonium dinitramide (ADN) monopropellant combustion with coupled condensed and gas phase kinetics. *Combust. Flame* **2014**, *161*, 347–362. [CrossRef]
77. Liau, Y.; Yang, V.; Lin, M.; Park, J. Analysis of ammonium dinitramide (ADN) combustion with detailed chemistry. In Proceedings of the 35th JANNAF Subcommitte Combustion Meeting, Tucson, AZ, USA, 7–11 December 1998.
78. Parr, T.; Hanson-Parr, D. Solid propellant diffusion flame structure. *Symp. (Int.) Combust.* **1996**, *26*, 1981–1987. [CrossRef]
79. Korobeinichev, O.P.; Paletsky, A.A. Flame structure of ADN/HTPB composite propellants. *Combust. Flame* **2001**, *127*, 2059–2065. [CrossRef]
80. Fujisato, K.; Habu, H.; Shibamoto, H.; Yu, X.; Miyake, A.; Hori, K. Combustion Characteristics of ADN (Ammonium Dinitramide) Based Solid Propellants. *Trans. Jpn. Soc. Aeronaut. Space Sci. Aerosp. Technol. Jpn.* **2012**, *10*, Pa89–Pa92. [CrossRef]
81. Wingborg, N.; Andreasson, S.; de Flon, J.; Johnsson, M.; Liljedahl, M.; Oscarsson, C.; Pettersson, A.; Wanhatalo, M., Development of ADN-Based Minimum Smoke Propellants. In Proceedings of the 46th AIAA/ASME/SAE/ASEE Joint Propulsion Conference & Exhibit, AIAA-2010-6586, Nashville, TN, USA, 25–28 July 2010; pp. 1–8. [CrossRef]
82. De Luca, L.T.; Shimada, T.; Sinditskii, V.P.; Calabro, M.; Manzara, A.P., An Introduction to Energetic Materials for Propulsion. In *Chemical Rocket Propulsion: A Comprehensive Survey of Energetic Materials*; De Luca, L.T., Shimada, T., Sinditskii, V.P., Calabro, M., Eds.; Springer International Publishing: Cham, Switzerland, 2017; pp. 3–59. [CrossRef]
83. Xue, T.; Liang, D.; Pang, W.; Shen, D.; Niamat, A.; Liu, J.; Zhou, J. Ignition and combustion of metal fuels under microgravity: A short review. *FirePhysChem* **2022**, *2*, 340–356. Progress in Solid Rocket Propulsion—Part B, [CrossRef]
84. Yetter, R.A.; Dryer, F.L., Metal Particle Combustion and Classification. In *Microgravity Combustion: Fire in Free Fall*; Ross, H.D., Ed.; Academic Press: San Diego, CA, USA, 2001; pp. 419–478.
85. Yetter, R.A.; Risha, G.A.; Son, S.F. Metal particle combustion and nanotechnology. *Proc. Combust. Inst.* **2009**, *32*, 1819–1838. [CrossRef]
86. Glassman, I.; Yetter, R.A.; Glumac, N.G. Chapter 9—Combustion of nonvolatile fuels. In *Combustion*, 5th ed.; Glassman, I., Yetter, R.A., Glumac, N.G., Eds.; Academic Press: Boston, MA, USA, 2015; pp. 477–536. [CrossRef]
87. Bucher, P.; Yetter, R.; Dryer, F.; Vicenzi, E.; Parr, T.; Hanson-Parr, D. Condensed-phase species distributions about Al particles reacting in various oxidizers. *Combust. Flame* **1999**, *117*, 351–361. [CrossRef]
88. Trunov, M.A.; Schoenitz, M.; Dreizin, E.L. Ignition of Aluminum Powders Under Different Experimental Conditions. *Propellants Explos. Pyrotech.* **2005**, *30*, 36–43. [CrossRef]
89. Price, E., Combustion of Metalized Propellants. In *Fundamentals of Solid-Propellant Combustion*; AIAA: Las Vegas, NV, USA, 1984; Chapter 9, pp. 479–513. [CrossRef]
90. Price, E.; Chakravarthy, S.; Freeman, J.; Sigman, R., Combustion of propellants with ammonium dinitramide. In Proceedings of the 34th AIAA/ASME/SAE/ASEE Joint Propulsion Conference and Exhibit, AIAA-98-3387, Cleveland, OH, USA, 13–15 July 1998; pp. 1–7. [CrossRef]
91. Pang, W.Q.; Fan, X.Z.; Zhang, W.; Xu, H.X.; Yan, N.; Xie, W.X.; Liu, F.L.; Wu, S.X. Effect of Ammonium Dinitramide (ADN) on the Characteristics of Hydroxyl Terminated Polybutadiene (HTPB) Based Composite Solid Propellant. *J. Chem. Sci. Technol.* **2013**, *2*, 53–60.
92. Gettwert, V.; Franzin, A.; Bohn, M.A.; De Luca, L.; Weiser, V. Ammonium Dinitrate/Glycidyl Azide Polymer (ADN/GAP) Composite Propellants with and without Metallic Fuels. *Int. J. Energetic Mater. Chem. Propuls.* **2017**, *16*, 61–79. [CrossRef]
93. De Luca, L.T.; Maggi, F.; Dossi, S.; Weiser, V.; Franzin, A.; Gettwert, V.; Heintz, T. High-energy Metal Fuels for Rocket Propulsion: Characterization and Performance. *Chin. J. Explos. Propellants* **2013**, *36*, 1–14.
94. De Luca, L.T.; Maggi, F.; Dossi, S.; Weiser, V.; Franzin, A.; Gettwert, V.; Heintz, T. New energetic ingredients for solid rocket propulsion. *J. Solid Rocket. Technol.* **2016**, *39*, 765–774.
95. Gogulya, M.; Makhov, M.; Dolgoborodov, A.; Brazhnikov, M. Detonation Performance of ADN and Its Mixtures with Al. In Proceedings of the Europyro 2003, Saint-Malo, France, 23–27 June 2003; pp. 18–27.
96. Price, D. Contrasting patterns in the behavior of high explosives. *Symp. (Int.) Combust.* **1967**, *11*, 693–702. [CrossRef]
97. Weiser, V.; Franzin, A.; Gettwert, V.; De Luca, L. Combustion of Metallised ADN/GAP Solid Rocket Propellants with Focus on Agglomeration Effects. In Proceedings of the Fifth European Conference for Aeronautics and Space Sciences (EUCASS), Munich, Germany, 1–5 July, 2013; pp. 1–10.
98. Volk, F.; Bathelt, H. *User's Manual for the ICT Thermodynamic Code*; Number v. 3 in Bericht/Fraunhofer-Institut für Chemische Technologie; ICT: Pfinztal, Germany, 1991.

99. Maggi, F.; Bandera, A.; Galfetti, L.; De Luca, L.T.; Jackson, T.L. Efficient solid rocket propulsion for access to space. *Acta Astronaut.* **2010**, *66*, 1563–1573. Private Human Access To Space, [CrossRef]
100. Weiser, V.; Franzin, A.; De Luca, L.T.; Fischer, S.; Gettwert, V.; Kelzenberg, S.; Knapp, S.; Raab, A.; Roth, E.; Eisenreich, N., Combustion Behavior of Aluminum Particles in ADN/GAP Composite Propellants. In *Chemical Rocket Propulsion: A Comprehensive Survey of Energetic Materials*; De Luca, L.T., Shimada, T., Sinditskii, V.P., Calabro, M., Eds.; Springer International Publishing: Cham, Switzerland, 2017; pp. 253–270. [CrossRef]
101. Gettwert, V.; Bohn, M.A.; Fischer, S.; Weiser, V. Performance of ADN/GAP Propellants Compared to Al/AP/HTPB. In Proceedings of the Insensitive Munitions & Energetic Materials Technology Symposium (IMEMTS), Rome, Italy, 18–21 May 2015; pp. 1–10.
102. Gettwert, V.; Tagliabue, C.; Weiser, V.; Imiolek, A. Green Advanced High Energy Propellants for Launchers (GRAIL)—First results on the Burning Behavior of AN/ADN Propellants. In Proceedings of the Sixth European Conference for Aeronautics and Space Sciences (EUCASS), Krakow, Poland, 29 June–3 July 2015; pp. 1–14.
103. Tagliabue, C.; Weiser, V.; Imiolek, A.; Bohn, M.A.; Heintz, T.; Gettwert, V. Burning Behaviour of AN/ADN Propellants. In Proceedings of the 47th International Annual Conference of the Fraunhofer ICT, Karlsruhe, Germany, 28 June–1 July 2016; pp. 1–15.
104. Gettwert, V.; Tagliabue, C.; Weiser, V. Burning Behavior of Aluminized ADN/PSAN Propellants. In Proceedings of the Seventh European Conference for Aeronautics and Space Sciences (EUCASS), Milan, Italy, 3–6 July 2017; pp. 1–9. [CrossRef]
105. Pozzoni, L.; Paravan, C.; Galfetti, L. ADN-based Formulations Analysis for Green Solid Propellants. In Proceedings of the Ninth European Conference for Aeronautics and Space Sciences (EUCASS), Lile, France, 9–13 July 2022; pp. 1–10. [CrossRef]
106. De Luca, L.T. Innovative Solid Formulations for Rocket Propulsion. *Eurasian-Chem.-Technol. J.* **2016**, *18*, 181–196. [CrossRef]
107. Tian, S.; Wang, Y.; Chen, X.; Hu, D.; Hu, Y.; Zheng, S.; Zhou, Z.; Xiao, C.; Ren, Z. Anti-hygroscopicity technologies for ammonium dinitramide: A review. *Propellants Explos. Pyrotech.* **2023**, *48*, e202200344. [CrossRef]
108. Gong, L.; Li, Y.; Guo, Y.; Li, J.; Yang, R. Effect of Morphology for Ammonium Dinitramide on the Mechanical and Combustion Properties of Composite Propargyl-terminated Copolyether Propellant. *Propellants Explos. Pyrotech.* **2020**, *45*, 864–870. [CrossRef]
109. Li, X.; Zhao, F.; Gao, H.; Yao, E.; Yi, J.; AN, T.; Hao, H.; Tan, Y. Preparation, characterization, and effects on thermal decomposition of ADN of nano Al/GAP composite particles. *Tuijin Jishu/Journal Propuls. Technol.* **2014**, *35*, 694–700.
110. Lin, X.; Zhao, F.; Luo, Y.; Gao, H.; Yao, E.; J., H. Solid phase chemical reduction synthesis and characterization of aluminium nanopowders and the effect on the thermal decomposition of ADN. *Rare Met. Mater. Eng.* **2015**, *44*, 1474–1478.
111. Lei, K.; Luo, Y.; Zhou, X.; Wang, Y.; Ma, T.; Jiang, X.; Wu, X.; Xu, S. Effects of micron-sized/nano-sized aluminum powder on the thermal safety characteristics of ammonium dinitramide under different types of thermal stimulations. *J. Therm. Anal. Calorim.* **2024**, 1–12. [CrossRef]
112. Li, J.; Tang, W.; Liu, Z.; Cong, K.; Gong, L.; Li, J.; Yang, R. Microsized aluminum/ammonium dinitramide core-shell particles to improve the combustion performance of aluminum powders. *J. Alloys Compd.* **2022**, *907*, 164349. [CrossRef]
113. Zhang, S.; Wang, J.; Feng, C.; Qiu, Y.; Ye, B.; Xu, C. Preparation of ADN-based energetic composite microspheres with excellent anti-moisture absorption and safety. *Chem. Eng. J.* **2024**, *494*, 153174. [CrossRef]
114. Qiao, S.; zhen Li, H.; wei Yang, Z. Decreasing the hygroscopicity of ammonium dinitramide (ADN) through cocrystallization. *Energetic Mater. Front.* **2022**, *3*, 84–89. [CrossRef]
115. Qiao, S.; Liu, Z.; Huang, S.; Wang, K.; Liu, Y.; Yang, Z. A novel ADN/TANPDO supramolecular crystal with anti-hygroscopicity and high energy: A promising strategy to construct advanced propellant materials. *Chem. Eng. J.* **2024**, *499*, 156152. [CrossRef]
116. Comet, M.; Schwartz, C.; Schnell, F.; Oudot, F.; Lallemand, B.; Spitzer, D. New Detonating Compositions from Ammonium Dinitramide. *Propellants Explos. Pyrotech.* **2021**, *46*, 742–750. [CrossRef]
117. Cristilli, F.; Weiser, V.; Maggi, F.; Imiolek, A.; Tagliabue, C.; Gettwert, V.; Dossi, S. Burning Behavior of ADN-Based Propellants Loaded with Al-Mg Mechanically Activated Powder. In Proceedings of the Seventh European Conference for Aeronautics and Space Sciences (EUCASS), Milan, Italy, 3–6 July 2017; pp. 1–10. [CrossRef]
118. Sims, S.; Fischer, S.; Tagliabue, C. ADN Solid Propellants with High Burning Rates as Booster Material for Hypersonic Applications. *Propellants Explos. Pyrotech.* **2022**, *47*, e202200028. [CrossRef]
119. Kore, R.U.; Kumar, N.; Vashishtha, A., Studying the Influence of Aluminium in ADN/HTPB based Solid Propellants. In Proceedings of the AIAA SCITECH 2024 Forum, AIAA-2024-1818, Orlando, FL, USA, 8–12 January 2024; pp. 1–14. [CrossRef]
120. Tian, Y.; Xu, W.; Cong, W.; Bi, X.; He, J.; Song, Z.; Guan, H.; Huang, C.; Wang, X. Research progress on the catalytic and thermal decomposition of ammonium dinitramide (ADN). *RSC Adv.* **2024**, *14*, 3636–3646. [CrossRef]
121. Fenn, J.; Raskino, M. *Mastering the Hype Cycle: How to Choose the Right Innovation at the Right Time*; Gartner Series; Harvard Business Press: Brighton, MA, USA, 2008.
122. A. Hahma, H.E.; Ostmark, H. The Properties of Ammonium Dinitramide (ADN): Part 2: Melt Casting. *J. Energetic Mater.* **2010**, *28*, 114–138. [CrossRef]

123. Rahm, M. Green Propellants. Doctoral thesis, KTH Chemical Science and Engineering, Royal Institute of Technology, SE-100 44, Stockholm, Sweden, 2010. Available online: https://www.diva-portal.org/smash/get/diva2:360054/FULLTEXT01.pdf (accessed on 31 December 2024).
124. Rahm, M.; Malmstrom, E.; Eldsater, C. Design of an ammonium dinitramide compatible polymer matrix. *J. Appl. Polym. Sci.* **2011**, *122*, 1–11. [CrossRef]
125. Ren, Z.; Chen, X.; Yu, G.; Wang, Y.; Chen, B.; Zhou, Z. Molecular simulation studies on the design of energetic ammonium dinitramide co-crystals for tuning hygroscopicity. *CrystEngComm* **2020**, *22*, 5237–5244. [CrossRef]
126. Zheng, S.; Wang, Y.; Hu, D.; Zhou, Z.; Xiao, C.; Tian, S.; Ren, Z. Cocrystallisation of high-energy oxidant ammonium dinitramide with triaminoguanidine nitrate for reduced hygroscopicity. *Chin. J. Chem. Eng.* **2024**, *74*, 249–258. [CrossRef]
127. Lu, Q.; Chen, F.; Xiao, L.; Yang, J.; Hu, Y.; Zhang, G.; Zhao, F.; Wang, Y.; Jiang, W.; Hao, G. Advances in the molecular simulation and numerical calculations of the green high-energy oxidant ADN. *Mater. Today Commun.* **2022**, *31*, 103699. [CrossRef]
128. Wang, J.; Cao, P.; Wang, X. Review of the Mechanical Properties and Numerical Simulation of Composite Solid Propellants. *Materials* **2023**, *16*, 6875. [CrossRef] [PubMed]
129. Kumar, T.; Jackson, T.L. Three-dimensional thermo-mechanical simulations of heterogeneous solid propellants. *Combust. Flame* **2021**, *233*, 111590. [CrossRef]
130. Ao, W.; Wen, Z.; Liu, L.; Liu, P.; Gan, Y.; Wang, L.; Li, L.K. Controlling the combustion and agglomeration characteristics of a solid composite propellant via a DC electric field. *Aerosp. Sci. Technol.* **2022**, *128*, 107766. [CrossRef]
131. Vijay, C.; Ramakrishna, P. Estimation of burning characteristics of AP/HTPB composite solid propellant using a sandwich model. *Combust. Flame* **2020**, *217*, 321–330. [CrossRef]
132. Fry, R.S. Solid Propellant Test Motor Scaling. Technical Report ADA395610, Chemical Propulsion Information Agency, Columbia, MD, 2001. Available online: https://apps.dtic.mil/sti/citations/ADA395610 (accessed on 31 December 2024).
133. Acket-Goemaere, A.; Brukardt, R.; Klempner, J.; Sierra, A.; Stokes, B. Space: The $ 1.8 Trillion Opportunity for Global Economic Growth. Mckinsey & Company. 2024. Available online: https://www.mckinsey.com/industries/aerospace-and-defense/our-insights/space-the-1-point-8-trillion-dollar-opportunity-for-global-economic-growth/ (accessed on 31 December 2024).
134. Daehnick, C.; Gang, J.; Rozenkopf, I. Space Launch: Are We Heading for Oversupply or a Shortfall? Mckinsey & Company. 2024. Available online: https://www.mckinsey.com/industries/aerospace-and-defense/our-insights/space-launch-are-we-heading-for-oversupply-or-a-shortfall (accessed on 31 December 2024).
135. Motta, F.; Pessoa Filho, J.B.; de Oliveira Moraes, A. Is there a market for micro-launch vehicles? *Space Policy* **2024**, *70*, 101629. [CrossRef]